Trafficking of nuclear-encoded apicoplast proteins depends on F-actin and Myosin F in *Toxoplasma gondii*

Parvathi Madhavi Devarakonda[a], Valeria Sarmiento[a], Aoife T. Heaslip [a, #]

[a] Department of Molecular and Cell Biology, University of Connecticut, Storrs, CT, 06269

Running Title: Protein trafficking to the apicoplast

[#]Address correspondence to Aoife Heaslip, aoife.heaslip@uconn.edu

ABSTRACT

Toxoplasma gondii contains an essential single plastid organelle known as the apicoplast that is necessary for fatty acid, isoprenoid, and heme synthesis. Perturbations affecting apicoplast function leads to parasite death. To maintain a functional apicoplast, the parasite must execute two important cellular processes: accurate division of this single copy organelle into daughter parasites during cell division and trafficking of nuclear encoded apicoplast proteins (NEAT). In this study we demonstrate that F-actin and an unconventional myosin motor, TgMyoF, are important for both processes. Live cell imaging demonstrates that during division the apicoplast is highly dynamic, exhibiting branched, U-shaped and linear morphologies that are dependent on TgMyoF and actin. These dynamics appear to control apicoplast association with the centrosome and positioning of the centrosome at the apicoplast tips. Loss of apicoplast dynamics correlated with reduced apicoplast-centrosome association and ultimately apicoplast inheritance defects. In addition, we uncovered the role of TgMyoF and actin in NEAT protein trafficking. Vesicles containing the apicoplast protein APT1 were only observed during apicoplast division in control parasites, however loss of TgMyoF and actin lead to accumulation of vesicles in the cytosol, with only a small impact on vesicle movement suggesting that this actomyosin system is important for vesicle fusion with the apicoplast. Consequently, loss of TgMyoF resulted in reduced apicoplast length. This study has provided crucial new insight into mechanisms and timing of protein trafficking to the apicoplast and demonstrated how apicoplast-centrosome association, a key step in the apicoplast division cycle, is control by the actomyosin cytoskeleton.

34 **INTRODUCTION**

35 The phylum Apicomplexa contains over 6,000 parasites, many of which are of significant
36 medical and veterinary importance, including *Toxoplasma gondii* the causative agent of
37 Toxoplasmosis and *Plasmodium spp*. which cause malaria [1]. These parasites are distinguished
38 by the presence of vestigial non-photosynthetic plastid organelle named the apicoplast
39 (Apicomplexan plastid), that is found in most Apicomplexa.

40 The apicoplast is an essential organelle required for fatty acid, isoprenoid, iron-sulfur
41 cluster and heme synthesis [2–8]. Genetic manipulations or perturbation of the apicoplast with
42 pharmacological compounds results in apicoplast inheritance defects and subsequently in parasite
43 death [9–11]. Despite containing a small 35kb genome, the majority of apicoplast localized
44 proteins including the proteins that are part of important biosynthetic pathways are encoded in the
45 nucleus. Therefore, trafficking of these proteins to the apicoplast is a critical cellular process and
46 our understanding of the mechanisms of apicoplast protein trafficking is incomplete. Many
47 apicoplast proteins contain a bipartite N-terminal signal sequence that includes a signal peptide
48 (SP), which directs protein translation to the endoplasmic reticulum (ER), and an apicoplast transit
49 peptide which is revealed after removal of the SP [12,13]. A subset of apicoplast proteins that
50 localize within the apicoplast membranes, including APT1, Atrx1 and FtsH1, are thought to traffic
51 using an alternate mechanism. These proteins do not contain a signal peptide or apicoplast
52 targeting sequences and have been observed in vesicles that are thought to directly traffic from the
53 ER to the apicoplast [14–18]. The molecular details of this trafficking system are poorly

54 understood, including timing and mechanisms of vesicle formation, transport and fusion with the
55 apicoplast.

56 Evolutionarily, the apicoplast was acquired by the parasite via a secondary endosymbiosis
57 of red algae and contains four membranes [19]. The inner two membranes are derived from the
58 progenitor chloroplast (inner most), the third from the algae plasma membrane (periplastid) and
59 outermost membrane from plasma membrane of the Apicomplexan ancestor which first acquired
60 this organelle (Fig. 1A). Protein translocons Tic and Toc in the inner two apicoplast membranes
61 facilitate protein transport from the periplastid to the apicoplast lumen [20,21]. Repurposed ER-
62 associated degradation (ERAD) proteins are thought to traffic proteins across the periplastid
63 membrane [22,23]. How proteins traverse the outer membrane is not understood but, in some
64 instances, may involve fusion of the outer membrane with ER derived vesicles [24].

65 The apicoplast is a single-copy organelle, thus apicoplast division and inheritance must
66 occur with high accuracy to ensure parasite survival. Apicoplast division is a multistep process.
67 During interphase the apicoplast has a circular morphology and is located at the parasite's apical
68 end (Fig. 1A). At the beginning of the cell division, the apicoplast interacts with the duplicated
69 centrosomes and elongates [25]. This interaction between centrosomes and the apicoplast is
70 dependent on the autophagy related protein Atg8 which localizes to the outer membrane of the
71 apicoplast and disruption of Atg8 in both *Toxoplasma* and *Plasmodium* results in apicoplast
72 inheritance defects [26–29]. While the apicoplast is elongated, daughter cell construction within
73 the parasite cytosol is initiated [30]. The apical tip of the growing daughters is connected to the
74 centrosomes via a fiber containing striated fiber assemblins (SFA) [31], ensuring that each

75 daughter cell inherits a single centrosome. As the centrosome migrates into the growing daughter
76 scaffolds, the elongated apicoplast then extends to a U-shaped structure, whereupon apicoplast
77 fission is mediated by dynamin related protein A (DrpA) [32].

78 Three cytoskeletal proteins, actin (TgAct1), Myosin F (TgMyoF: an unconventional
79 apicomplexan specific myosin motor), and the actin nucleator formin-2 also play major roles in
80 apicoplast division [33–36]. However, the field lacks a clear understanding of the specific steps of
81 apicoplast division mediated by this actomyosin system. In addition to their roles in apicoplast
82 division, TgMyoF and actin control the transport of a variety of vesicles, including dense granules
83 and Rab6 vesicles [36,37], although their role in trafficking vesicles destined for the apicoplast has
84 not been investigated.

85 In this study, we further define the roles of TgMyoF and actin in apicoplast division and
86 apicoplast vesicle trafficking. We show that loss of TgMyoF and actin led to an accumulation of
87 apicoplast-destined vesicles in the cytosol. However, loss of these proteins only had a minor
88 impact on vesicle movement suggesting a function in vesicle fusion with the outer membrane of
89 the apicoplast. Live cell imaging also revealed that elongated apicoplasts are highly dynamic,
90 exhibiting linear, branched and U-shaped morphologies which are driven by both TgMyoF and
91 actin. Loss of this actomyosin system results in reduced apicoplast length and defects in apicoplast-
92 centrosome association which ultimately leads to defects in apicoplast inheritance.

93 **MATERIAL AND METHODS**

94 **Cell culture**

95 RH parasites were maintained by passage in human foreskin fibroblast (HFF) cells obtained from
96 ATCC (Catalog # CRL-2429). HFFs were grown to confluence in Dulbecco's modified Eagle's
97 medium containing 10% (v/v) heat inactivated fetal bovine serum (FBS) and 1% (v/v)
98 antibiotic/antimycotic at 37°C, 5% CO_2. Before parasite addition, confluent HFF monolayers were
99 maintained in Dulbecco's modified Eagle's medium containing 1% (v/v) heat inactivated fetal
100 bovine serum (FBS) and 1% (v/v) antibiotic/antimycotic 37°C, 5% CO_2.

101 **Drug treatment**

102 *Cytochalasin D treatment*. For fixed cell imaging, parasites invaded confluent HFF monolayer for
103 4 hours and then treated with 0.2 μM cytochalasin D (CD) or equivalent volume of DMSO for 12
104 hours before fixation with 4% paraformaldehyde. For live cell imaging, parasites were grown for
105 12 hours before treatment with 2 μM CD or equivalent volume of DMSO for 30 minutes. Imaging
106 was carried out in the presence of DMSO or CD.

107 *IAA Treatment*: To deplete TgMyoF protein levels, *TgMyoF-mAID:TgAPT1-EmGFP* parasites
108 were grown in confluent HFF monolayer for 5 or 12 hours and then treated with a final
109 concentration of 500 μM indole acetic acid (IAA) or equivalent volume of 100% ethanol for 6 or
110 15 hours before fixation for immunohistochemistry or live cell imaging [38,39].

111 **Creation of transgenic parasite lines**

112 A list of parasite lines, primers and gene accession numbers used in this study can be found in
113 Tables 1, 2 and 3 respectively.

114 *Parasite transfection*

115 Parasite transfection was conducted as previously described [40]. Briefly, linearized or circular
116 plasmid DNA or CRISPR HR oligo (produced by PCR) was ethanol precipitated, washed twice
117 70% ethanol pre-chilled to -20°C and resuspended in cytomix (120mM KCl, 10mM potassium
118 phosphate (pH 7.6), 25mM HEPES (pH 7.6), 2mM EGTA (pH 7.6), 5mM $MgCl_2$, 2mM potassium
119 ATP, 150uM $CaCl_2$, 5mM reduced glutathione) and electroporated using a BTX electroporator set
120 as follows: voltage 1500 V, capacitance 25 µF and resistance 25 Ω.

121 *Creation of TgAPT1-EmGFP parasite line*

122 In the *TgAPT1-EmGFP* parasite line the endogenous TgAPT1 gene is tagged with EmeraldGFP
123 (EmGFP). The pTKOII_APT1EmGFP plasmid was created from pTKOII_MyoF-EmGFP
124 plasmid [37] by digesting with AvrII and BglII restriction enzymes to remove the TgMyoF
125 genomic sequence. 2 kb of genomic DNA upstream of the TgAPT1 stop site was amplified by
126 PCR using Q5 high fidelity polymerase (New England BioLabs) using the Ku80 genomic DNA
127 as a template and the primers TgAPT1 F1 and TgAPT1 R1 (Table 2). The plasmid backbone and
128 the PCR product were gel purified. Ligation of the plasmid was carried out via Gibson assembly
129 using NEB builder HiFi DNA assembly master mix as per manufacturer's instructions (New
130 England Biolabs; catalog # M5520AA2) and transfected into NEB5α bacteria. Positive clones
131 were screened by colony PCR and verified by sanger sequencing. pTKOII-TgAPT1-EmGFP
132 plasmid was linearized for homologous recombination using the PstI restriction enzyme and
133 25µg was transfected into $1x10^7$ *ΔKu80: ΔHXGPRT* parental parasites [41,42]. 24 hours after
134 transfection mycophenolic acid in ethanol and Xanthine in 0.3M NaOH were added to growth
135 media to a final concentration of 25µg/ml and 50µg/ml respectively. Drug treatment continued

136 until at least 75% of the parasites were EmGFP positive. Clonal parasites lines were FACS
137 sorted into a single 96-well plate (2 per well) and grown for 7 days to isolate clonal parasite lines
138 resulting in the creation of TgAPT1-EmGFP parasite line. To verify integration of this construct
139 into the APT1 genomic locus, genomic DNA was isolated using Qiagen DNeasy blood and
140 tissue kit as per manufacturer's instructions (Qiagen, Germantown, MD) and confirmed via PCR
141 using the primers TgAPT1-Promoter F1, APT1 CDS R, EmGFP R (Table 2) (Fig. S1).

142 *Creation of TgMyoF-mAID; TgAPT1-EmGFP parasite line*

143 In the *TgMyoF-mAID:TgAPT1-EmGFP* parasite line, the endogenous TgMyoF gene is tagged with
144 HA-mAID [37] and TgAPT1-EmGFP is expressed under the control of the APT1 promoter from
145 the dispensable UPRT locus. For the creation of 5'UPRT-pAPT1-APT1-EmGFP-3'UPRT
146 plasmid (which will be used as a template for created of the HR oligo via PCR), 5'UPRT-pMyoF-
147 mcherry-TgMyoF-3'UPRT (unpublished plasmid) was digested with AvrII and AflII restriction
148 enzyme to remove the pMyoF-TgMyoF-mcherry sequence and replace with pAPT1-TgAPT1-
149 EmGFP fragment, containing 1Kb of upstream of the APT1 start codon and the APT1 coding
150 sequence. TgAPT1-EmGFP sequence was amplified from the pTKOII_APT1-EmGFP plasmid
151 and primers 5'-APT1-UPRT-F and 3'-APT1-UPRT-R (Table 2). The plasmid backbone and the
152 PCR product were gel purified. Ligation of the plasmid was carried out via Gibson assembly as
153 per manufacturer's instructions (New England Biolabs; catalog # M5520AA2) and transfected into
154 NEB5alpha bacteria. Positive clones were screened by colony PCR and verified by sanger
155 sequencing.

156 The CRISPR HR oligo was generated by PCR using UPRT F and UPRT R primers and
157 the 5'UPRT-pAPT1-APT1-EmGFP-3'UPRT plasmid as a template with Q5 high fidelity
158 polymerase and50ul of PCR reaction was cotransfected with 25 μg of pSag1::Cas9::U6::sgUPRT
159 plasmid [43] (AddGene plasmid # 54467) into $1x10^7$ TgMyoF-mAID parasites [37]. 24 hours
160 post-transfection parasites were treated with 10 μM fluorodeoxyribose (FUDR) (which selects
161 for loss of the UPRT gene [44]) until at least 75% of the parasites were EmGFP positive.
162 Parasites were FACS sorted for EmGFP positivity into a single 96-well plate (2 per well) and
163 grown for 7 days. Single clones were selected for further analysis. Genomic DNA was isolated
164 using Qiagen DNeasy blood and tissue kit as per manufacturer's instructions (Qiagen,
165 Germantown, MD). Genomic DNA was analyzed for correct insertion into the UPRT locus via
166 PCR using primers 5'-UPRT F, APT1 CDS R and UPRT-Intron R (Table 2) (Fig. S2).
167 *Creation of ectopic ATG8 expression plasmid*
168 Generation of pAtg8-3xTy-Atg8 plasmid for ectopic expression of TgAtg8 under the endogenous
169 promoter was a 2-step process. First, we created the pAtg8-tdTomato-Atg8 plasmid by digesting
170 the pTub_tdTomato-Atg8 [26] with SfoI and BglII restriction enzymes to remove the tubulin
171 promoter sequence. TgAtg8 promoter was amplified from the Ku80 parental genomic DNA using
172 the primers Atg8 promoter F and Atg8 promoter R. Plasmid backbone and the PCR product was
173 gel purified. Ligation of the plasmid was carried out via Gibson assembly as per manufacturer's
174 instructions (New England Biolabs; catalog # M5520AA2) and transfected into NEB5alpha
175 bacteria. Positive clones were screened by colony PCR using Atg8 promoter F and Atg8 promoter
176 R (Table 2) and verified by sanger sequencing. In the second step, pAtg8-tdTomato-Atg8 was
177 digested with AvrII and BglII restriction enzymes to remove tdTomato coding sequence. The3xTy

178 tag was created by PCR using primers 3xTy F and 3xTy R (Table 2) and the pTKOII_MyoL-3xTy-
179 mAID plasmid as a template (unpublished plasmid; Table 1). Ligation of the plasmid with 3Xty
180 insert was carried out via Gibson assembly as per manufacturer's instructions (New England
181 Biolabs; catalog # M5520AA2) and transfected into NEB5alpha bacteria. Positive clones were
182 screened by colony PCR using primers Atg8 promoter F and 3xTy R and verified by sanger
183 sequencing.25 µg of the pAtg8-3xTy-Atg8 plasmid was transiently transfected into the TgMyoF-
184 mAID parasite line and were grown for 12h before treating the parasites with either ethanol or
185 IAA for 6h.

186 **Fluorescence microscopy**

187 All live and fixed images were acquired on a DeltaVision Elite microscope system built on an
188 Olympus base with a 100x 1.39 NA objective in an environmental chamber heated to 37 ˚C. This
189 system is equipped with a 15-bit scientific CMOS camera and DV Insight solid state illumination
190 module with excitation wavelengths DAPI = 390/18nm, FITC = 475/28nm, TRITC = 475/28nm
191 and Alexa 647 = 632/22nm. Single band pass emission filters had the following wavelengths DAPI
192 435/48nm, FITC = 525/48nm, TRITC = 597/45nm and Alexa 647 = 679/34nm. Image acquisition
193 speeds for the live cell imaging were determined on a case-by-case basis and are indicated in the
194 figure legends. All cells were imaged in multiple focal planes and Z-series were captured at 0.2
195 µm (fixed) or 0.4 µm (live) steps. Images presented in the figures represent maximum intensity Z-
196 slice projections. Brightness and contrast of images were optimized for print.

197 **Immunocytochemistry and live cell imaging**

198 Parasites were fixed with freshly made 4% paraformaldehyde (Electron microscopy
199 sciences, Catalog # 15714) in 1x PBS for 15 minutes at room temperature. Cells were washed three
200 times in 1x PBS and permeabilized in 0.25% Triton X-100 (ThermoFisher) in 1x PBS for 15
201 minutes at room temperature. Cells were washed three times in 1x PBS and were blocked in 2%
202 BSA in 1x PBS and incubated for 15 minutes. All antibodies were diluted in 2% BSA/1x PBS at
203 the concentrations listed in the Table 4. Cells were incubated sequentially with primary and
204 secondary antibody at room temperature for 30 minutes each, with 3 washes with 1x PBS between
205 incubations. To stain DNA parasites were incubated in 10 µM DAPI diluted in 1x PBS for 10
206 minutes and then washed three times in 1x PBS. Coverslips were mounted onto slides using either
207 Prolong Gold (ThermoFisher Catalog # P36930) or Prolong diamond (ThermoFisher Catalog #
208 P36970) anti-fade reagent and allowed to dry overnight before imaging.

209 Growth media was replaced with Fluorobrite DMEM (ThermoFisher) containing 1% FBS
210 and 1x antimycotic/antibiotic pre-warmed to 37 ˚C before live cell imaging.

211 **Image analysis**

212 *Quantification of TgAPT1 Vesicle number*

213 To determine the number of APT1 vesicles during parasite division. The apicoplasts were
214 categorized according to their morphology to distinct stages of apicoplast division stage
215 (interphase, elongation, and post fission) by visualizing apicoplast morphology with anti-Cpn60
216 IFA and expression of TgAPT1-EmGFP. Cell cycle stage by determined by expressing ptub-
217 mCherry-TubulinA1 a marker for the pellicle of daughter and mother parasites. Number of vesicles

218 were counted manually on average intensity projection images using cell counter plugin in Fiji
219 (Fiji is Just ImageJ; http://imageJ.net). Three independent experiments were performed with 25
220 parasites per experiment counted for each stage of division.

221 *Characterization of TgAPT1 vesicle motion*

222 To characterize TgAPT1 vesicle motion, vesicle tracking analysis was performed using Imaris
223 v9.9.0 microscopy image analysis software (Bitplane AG, Oxford Instruments). Z-stack movies
224 that were bleach corrected in ImageJ using the histogram matching algorithm were uploaded to
225 Imaris and brightness and contrast was auto-adjusted using the "normalize time point" extension.
226 Movies were cropped to remove areas that did not contain apicoplast and vesicles. To prevent
227 aberrant tracking inside the apicoplast itself, the apicoplasts were demarcated from vesicles using
228 the surface tool with a lower surface threshold of 1500 arbitrary units (a.u.). Vesicles were
229 identified using the spots creation wizard. Size parameter (estimated XY diameter) was 0.3 µm.
230 To distinguish between vesicles and background fluorescence, only objects with a fluorescence
231 intensity above 150 a.u. were tracked. Tracks were created using autoregressive motion algorithm.
232 To be considered true vesicles, vesicles must be located within 5 µm from the apicoplast surface.
233 A maximum gap of 2 frames was permitted, (i.e., maximum number of the consecutive time points
234 that a track segment can be missed to be considered continuous). Tracks with less than 5 data
235 points were excluded from the analysis as it was not possible to accurately assign a straightness
236 value. Two independent experiments with a total of 14-17 videos were used for this analysis.
237 Straightness values were calculated by determining the ratio of track displacement (the distance
238 between first and last positions of the vesicle) to track length (total distance traveled).

239 *Measuring apicoplast to centrosome distance*

240 Distance between the elongated apicoplast and centrosomes was determined using the straight-line
241 tool in ImageJ by measuring the closest distance from each centrosome to the apicoplast. The
242 distance was considered as 0 when there was an overlap between fluorescence pixels in each
243 channel. Three independent experiments were performed (N=108 and 93 from control and
244 knockdown respectively).

245 *Measuring apicoplast length*

246 Elongated apicoplast length was measured using segmented/straight line tool in Fiji. Three
247 independent experiments were performed (N=60 parasites total).

248 *Daughter cell-apicoplast proximity categories*

249 For determining the apicoplast proximity to growing daughter cells, we visualized apicoplast
250 localization (Cpn60 staining) in growing daughter parasites (based on eGFP-tubulin). Daughter
251 proximity to the apicoplast was determined visually and categorized as being near to both the
252 daughters (2D), near to one of the daughters (1D) or not close to either daughter (none). Three
253 independent experiments were performed (N=60 total).

254 *TgAtg8 localization*

255 TgAtg8 localization during different stages of apicoplast division was determined using anti-Ty
256 antibody staining (kind donation of Dr. Chris de Graffienried: Brown University). Two
257 independent experiments were performed (25 parasites per experiment).

258 **Statistical analysis**

259 Statistical analysis was performed using GraphPad Prism software. Statistics on data sets were
260 performed using unpaired t-tests. P-values <0.05 were considered statistically significant.
261 Superplots were made as described in Lord et al., [45].

262 **RESULTS**

263 **The number of TgAPT1-EmGFP vesicles in the cytosol increases during apicoplast**
264 **elongation**

265 To investigate the mechanisms of apicoplast division and apicoplast protein trafficking from the
266 ER, we generated a parasite line where the endogenous TgAPT1 gene was tagged with EmGFP
267 (Emerald green fluorescent protein) (Fig. 1A and 1B; Fig S1) as TgAPT1 was previously observed
268 localizing to vesicles in the parasite cytosol and the apicoplast [15,46]. To demarcate the parasite
269 periphery and enable quantification of vesicle number at each stage of the parasite division cycle,
270 mCherry-TubulinA1 was transiently expressed in parasites for ~18h prior to fixation and staining
271 with anti-Cpn60 antibody, a marker of the apicoplast stroma. Based on the apicoplast shape and
272 the presence and size of daughters, parasites were categorized as interphase (no daughter parasites,
273 circular apicoplast), elongating (small daughters, elongated apicoplast) or post-fission (large
274 daughters, circular apicoplast in each daughter) and the number of vesicles per parasite was
275 determined at each cell cycle stage. In interphase parasites, TgAPT1 forms a ring that surrounds
276 the TgCpn60 signal consistent with its localization at the apicoplast membrane (Fig. 1B) and the
277 number of TgAPT1 positive (TgAPT1+) vesicles per parasite is low (1.15±0.07, mean±SEM) (Fig.
278 1B and 1C). During elongation, the number of TgAPT1 vesicles in the cytosol increased 7-fold to

279 8.08±0.5 vesicles per parasite (Fig. 1B and 1C). After apicoplast fission and segregation into the
280 daughter cells, the number of TgAPT1 vesicles per parasite decreased to 3.68±0.2 (Fig. 1B and
281 1C). This data demonstrates that the vesicle trafficking to the apicoplast is cell cycle dependent
282 and occurs predominantly during apicoplast elongation. Interestingly, Cpn60, a nuclear encoded
283 protein that localizes to the apicoplast stroma, was not found in TgAPT1+ vesicles (Fig. 1B, inset).

284 **Actin depolymerization and TgMyoF knockdown leads to increased number of TgAPT1-**
285 **EmGFP vesicles in the cytoplasm**

286 TgACT1 and TgMyoF are cytoskeletal proteins with previously established roles in vesicle
287 transport [36,37]. Therefore, we wanted to determine if these proteins play a role in vesicle
288 trafficking to the apicoplast. To do this a previously generated auxin inducible TgMyoF
289 knockdown parasite line TgMyoF-mAID [37] was modified to express TgAPT1-EmGFP under
290 the endogenous TgAPT1 promoter from the dispensable UPRT locus to create TgMyoF-
291 AID/TgAPT1-GFP parasite line (Fig. S2A).

292 To knockdown TgMyoF, TgMyoF-AID; TgAPT1-GFP parasites were treated for 15 hours
293 with ethanol (control) or 500 μM IAA, which results in depletion of TgMyoF to undetectable
294 levels after 4 hours [37]. To depolymerize actin, TgAPT1-EmGFP parasites were treated with
295 DMSO (control) or 0.2 μM cytochalasin D (CD) for 12h prior to fixation. Parasites transiently
296 expressing mCherry-Tubulin were categorized as interphase, elongation or post-fission as
297 described for figure 1. Both actin depolymerization and TgMyoF depletion resulted in an
298 approximately 2-fold increase in the number of TgAPT1-EmGFP positive vesicles at all stages of
299 the apicoplast division (Fig. 2A-F; Fig. S3 & S4). In both treatment conditions, an apicoplast

300 inheritance defect was observed as expected [35] (Fig. 2A&2D; magenta arrow). "Apicoplast-less"
301 parasites contained the highest accumulation of vesicles in comparison to all other stages of
302 apicoplast division (Fig. 2C and F).

303 **TgAPT1 vesicles exhibit predominately diffusive-like motion**

304 Next, we sought to describe the motion characteristics of TgAPT1+ vesicles, as the
305 previous work demonstrated that other vesicle types within the parasite including dense granules,
306 Rab6+ and Rop1+ vesicles were transported throughout the parasite cytosol in an actin and
307 TgMyoF dependent manner [36,37]. TgAPT1-EmGFP parasites in the elongation phase of
308 apicoplast division were imaged by live cell microscopy. Visual inspection of these recordings
309 revealed two striking observations. First, TgAPT1-EmGFP vesicles were found in the parasite
310 cytosol, confirming observations from the fixed cell experiments (Fig. 1 and 2). The motion of
311 these vesicles was predominately diffusive (Fig 3A; inset 2), although a small number of vesicles
312 exhibited directed motion, i.e., – sustained movement in a single direction for continuous frames
313 (Fig. 3A; inset 1) (Video S1). Secondly, elongated apicoplasts was not static, linear structures, but
314 exhibited changes in morphology throughout the 2-5min imaging period (Fig. 4; Video S2).

315 To quantify vesicle movement in an automated and unbiased manner, vesicle motion
316 analysis was performed using spot creation wizard Imaris microscopy image analysis software
317 (https://imaris.oxinst.com/)(Fig. 3B). To prevent aberrant vesicle tracking inside the fluorescently
318 labeled apicoplast a surface mask was created over the apicoplast itself (Fig 3B; raw vs. surface).
319 Vesicles were automatically detected based on size and fluorescent intensity (Fig. 3B; surface and
320 vesicles) (See materials and methods for details). Vesicles that are transported in an active, motor

321 driven manner typically exhibit "directed trajectories", i.e.-vesicles move in approximately a
322 straight trajectory [36], while diffusive vesicles exhibit random movements. Thus, to determine
323 the number of vesicles exhibiting diffusive or directed movement track straightness was calculated
324 by determining the ratio of track displacement (the distance between first and last positions of the
325 vesicle) to track length (total distance traveled). A straightness value close to zero indicates random
326 motion, i.e. – track length is greater than the distance between the first and last positions indicating
327 random motion. A straightness value close to 1 indicates that the total distance travelled and the
328 distance between the first and last positions were similar indicating that the vesicle moved in
329 approximately a straight line. Vesicle tracks observed in the first 20 seconds of imaging are color
330 coded according to straightness (Fig. 3B). A frequency distribution of the straightness values
331 indicates that over 80% of vesicles have a straightness value less than 0.5 and a mean straightness
332 value was 0.17±0.15 confirming that apicoplast vesicle motion is predominantly diffusive in nature
333 (Fig. 3C). We then compared the track displacement length for trajectories that had a straightness
334 value greater or less than 0.5. Randomly moving vesicles (with a straightness value <0.5) had a
335 mean track displacement value of 0.3μm. While vesicles with straighter trajectories moved twice
336 as far with a mean displacement of 0.59 μm (Fig. 3D).

337 **TgAPT1-EmGFP vesicle motion is dependent on TgMyoF and Actin**

338 Next, we sought to determine if actin depolymerization or TgMyoF knockout altered
339 vesicle motion. TgAPT1-EmGFP parasites were grown for 18h prior to treatment with 2 μM CD
340 or equivalent volume of DMSO for 30 min before live cell imaging (Fig. 3E) (Video S3), while to
341 deplete TgMyoF, TgMyoF-AID; APT1-EmGFP parasites were grown for 15 hours with ethanol
342 or 500μm IAA before live cell imaging (Fig. 3F) (Video S4).

343 Vesicles movements were again tracked with Imaris as described above. Actin
344 depolymerization or TgMyoF knockout had no effect on the mean straightness values for DMSO,
345 CD, Ethanol and IAA treated parasites were 0.18±0.18, 0.14±0.13, 0.2±0.17 and 0.17±0.17
346 respectively (Fig. 3G and 3H). Although, upon loss of F-actin and TgMyoF, the number of vesicles
347 in the cytosol was increased compared to controls. In all cases (treatment and control) the
348 percentage of vesicles with a straightness value <0.5 was ~80%. To determine if the movement of
349 the remaining ~20% of vesicles was TgMyoF and actin driven, vesicles with a straightness value
350 greater than 0.5 were analyzed further. Since vesicles with a straightness value with greater than
351 0.5 exhibited longer track displacement (Mean length was 0.59µm (Fig. 3D)) we defined "directed
352 trajectories" as those with a straightness value >0.5 and a track displacement length of at least
353 0.5µm. In no treatment, DMSO- and ethanol-treated parasites, the percentage of vesicle which met
354 these criteria were 9.5%, 10.3% and 11% for respectively. Upon actin depolymerization with CD
355 or TgMyoF knockdown this percentage was significantly reduced to 4.7% and 6.8% respectively
356 (Fig. 3I).

357 **The apicoplast undergoes morphological changes during elongation**

358 Live cell imaging of TgAPT1-EmGFP parasites also demonstrated that the apicoplast
359 morphology in the elongation phase of apicoplast division was highly variable between individual
360 vacuoles. In some vacuoles, the apicoplast appeared to be highly dynamic exhibiting alternating
361 linear, U-shaped and branched morphologies throughout the ~2-minute imaging period (Fig. 4A;
362 top panel) (Video S2), while others were static in the elongation phase of apicoplast division
363 (Figure 4A; bottom panel) (Video S2). Given this variability, we quantified the percentage of
364 apicoplasts that were highly dynamic and exhibited rapid changes in morphology during the course

365 of imaging (102 seconds) (Fig. 4A and B). ""Dynamic" apicoplasts were defined as those that
366 exhibited one or more of the following morphological changes: extending and/or retracting,
367 bending, or branch formation, or branch movement (Fig. 4A; top panel). 63±6.1% (Mean±SEM)
368 of the apicoplasts were highly dynamic (Fig. 4B). Whereas 37±6.1% (Mean±SEM) of parasites
369 contained either less dynamic apicoplasts, exhibiting subtle changes in morphology during the
370 course of live cell imaging, or were static with no observable changes in the morphology
371 throughout the ~2-minute imaging time (Fig 4A and B).

372 **Apicoplast dynamics requires actin and TgMyoF proteins**

373 Considering the dynamic nature of the apicoplast, we wanted to determine if these
374 dynamics are dependent on actin and TgMyoF. To depolymerize actin, TgAPT1-EmGFP parasites
375 were again treated with 2 μM cytochalasin D or equivalent volume of DMSO for 30 min before
376 live cell imaging (Fig. 4C). 82±2.9% (Mean±SEM) of the apicoplasts in control DMSO-treated
377 parasites were highly dynamic, while only 9±6.6% (Mean±SEM) of the apicoplasts in the
378 cytochalasin D treated parasites were highly dynamic (Fig. 4D). To test the role of TgMyoF in
379 apicoplast dynamics, TgMyoF-mAID; TgAPT1-EmGFP parasites treated with 500 μM indole
380 acetic acid (IAA) to induce TgMyoF knockdown for 15h prior to live cell imaging (Fig. 4E).
381 Similar to the cytochalasin D treatment, TgMyoF knockdown resulted in reduced apicoplast
382 dynamics. The percentage of parasites with a highly dynamic apicoplast was significantly reduced
383 from 86±4% (Mean±SEM) in control parasites to 22±13% in the TgMyoF KD parasites (Fig. 4F).

384 **The apicoplast dynamically associates with static centrosomes**

385 Apicoplast association with the centrosomes is a crucial step in the apicoplast division
386 cycle. In the first step in the cell division cycle, the centrosome migrates to the basal end of the
387 nucleus and duplicates, then both centrosomes return to the apical side of the nucleus where they
388 associate with the apicoplast [25,47]. The dynamics of the elongated apicoplast have not
389 previously been described and it is unclear if or how the apicoplast's interaction with the
390 centrosomes, which are embedded in the nuclear envelope [48], is maintained during apicoplast
391 movement.

392 To further explore this phenomenon, wild type parasites were transiently transfected with
393 plasmids containing FNR-RFP (a marker for the apicoplast; [25]) and Centrin 1-GFP expression
394 cassettes and visualized using live-cell microscopy [49]. In parasites with highly dynamic,
395 elongated apicoplasts the centrosomes were not always associated with the tips of the apicoplast
396 but were frequently associated with the sides of the elongated apicoplast (Fig. 5A; inset 1 and 3)
397 (Video S5). The apicoplast appears to slide in relation to the static centrosome (Fig. 5A, Inset 1,
398 Video S6). The apicoplast was observed to undergo branching when the centrosome was
399 associated with the side rather than the tip of the apicoplast (Fig. 5A; Inset 3, magenta arrow)
400 (Video S7). The most dramatic morphological changes occurred when the apicoplast was
401 associated with only a single centrosome (Figure 5A, Inset 2). The apicoplast was observed
402 extending towards the second centrosome before retracting backwards. In contrast to the dynamics
403 observed in the elongation phase of apicoplast division, interphase and post-fission apicoplasts
404 were static. In interphase parasites the apicoplast was circular and did not change shape over the
405 course of imaging (Fig. 5B; upper panel) (Video S8). After apicoplast fission, the apicoplast

406 remains elongated for a time before retraction into a circular morphology. Post-fission elongated
407 apicoplasts are static over the course of the imaging period. The apicoplast movement and
408 branching that were observed prior to fission are no longer observed and centrosomes are statically
409 associated with the apicoplast tips (Fig. 5B; lower panel) (Videos S9).

410 TgMyoF knockdown results in the disruption of the apicoplast and centrosome 411 interaction

412 It has previously been demonstrated that loss of TgMyoF affects centrosome positioning
413 and the orientation of daughter cell growth within the mother resulting in a high number of "upside
414 down" daughter parasites [35]. However, "upside down" daughters are also observed in wildtype
415 parasites ([35]; Fig 6), and so it is unclear why the apicoplast fails to be inherited by "upside down"
416 parasites in the TgMyoF knockout. Our live cell imaging of apicoplast and centrosome
417 interactions, suggest that apicoplast dynamics are important for initiating the interaction between
418 these two structures and positioning of the centrosomes at the apicoplast tips. Therefore, we
419 directly investigated if the loss of TgMyoF, which disrupted apicoplast dynamics (Fig. 4), also
420 disrupted apicoplast-centrosome interactions. TgMyoF-mAID parasites transiently expressing the
421 centrosome marker GFP-Centrin1 were grown for 12 hours post invasion and then treated with
422 ethanol or 500 μM IAA for 6 hours before fixation. This shortened IAA treatment time compared
423 with previous experiments allowed us to visualize the apicoplast and centrosomes in the first cell
424 division cycle after depletion of TgMyoF. Parasites were stained with an anti-Cpn60 antibody to
425 mark the apicoplast and an anti-IMC1 antibody to mark the pellicle of both mother and daughter
426 parasites. In control parasites, the centrosomes are associated with either the sides or the tips of

427 the apicoplast (Fig. 6A). However, in TgMyoF knockout parasites, which contain daughter
428 parasites comparable in size to the daughters in control parasites, two out of four parasites
429 contained an apicoplast that was associated with only a single centrosome (Fig. 6A; inset).
430 Quantification of the distance between the elongated apicoplast and the centrosomes revealed that
431 the average distance between the centrosome and apicoplast increased by 50% from 0.44±0.05 µm
432 (Mean±SEM) in control parasites to 1.03±0.08 µm in TgMyoF knockout parasites (Fig. 6B) and
433 only 24% of centrosomes associated with the apicoplast in TgMyoF knockdown parasites
434 compared to 55% in controls.

435 We next assessed how this loss of centrosome interaction affected apicoplast inheritance.
436 Elongated apicoplasts in 100% of control parasites were found to be in close proximity to both of
437 the growing daughter parasites. In early stages of division, the apicoplast was adjacent to the
438 daughter parasites (Fig. 7C; white arrow head). Later in division, both daughters contain one end
439 of the elongated apicoplast, even when one the daughters was in the "upside down" orientation
440 (Fig 7C; magenta arrowhead). Upon depletion of TgMyoF only 13.3% of elongated apicoplasts
441 were in close proximity to both the growing daughter parasites (2D) while 70% of the elongated
442 apicoplasts were in close proximity to only one of the daughter parasites (1D) (Fig. 6C; white
443 arrow), and 16.6% of the elongated apicoplasts were not found to be in close proximity to either
444 of the growing daughter parasites (none) (Fig. 6D and Fig. S5). Thus, the disruption of the
445 centrosome-apicoplast interaction leads to asymmetric segregation of the apicoplast into a single
446 daughter cell or to the residual body.

447 **TgMyoF knockdown did not alter TgAtg8 localization with the apicoplast**

448 Previously, it has been shown that TgAtg8 localizes to the apicoplast and that the loss of
449 TgAtg8 disrupts the interaction between centrosomes and the elongated apicoplast resulting in
450 asymmetric distribution of elongated apicoplast to the growing daughter parasites, reminiscent of
451 the phenotype observed after TgMyoF depletion (Fig. 6A-D) [26]. To determine if loss of TgMyoF
452 affected the localization of TgAtg8 at the apicoplast, TgMyoF-mAID parasites transiently
453 expressing TgAtg8-3xTy under the endogenous TgAtg8 promoter were treated with ethanol or 500
454 μM IAA for 6h before fixation and staining with anti-Cpn60 antibody. TgAtg8 localized to the
455 apicoplast at all stages of the apicoplast division cycle and knockdown of TgMyoF did not disrupt
456 TgAtg8 localization (Fig. 6E and Fig. S6) indicating that the loss of interaction between
457 centrosomes and the elongated apicoplast seen in the TgMyoF knockdown parasites is not due to
458 mislocalization of TgAtg8.

459 **TgMyoF knockdown results in reduced apicoplast length**

460 Depolymerization of actin and knockdown of TgMyoF resulted in reduced apicoplast
461 dynamics (Fig. 4) and increased accumulation of TgAPT1 vesicles (Fig. 2. Since loss of these
462 proteins only had a minor impact on vesicle movement (Fig. 3), this data suggests that actin and
463 TgMyoF play a role in TgAPT1 vesicle fusion with the apicoplast that would thereby limit the
464 addition of new material (proteins and lipids) needed for a doubling of apicoplast contents before
465 fission. Therefore, we accessed apicoplast length in the elongation phase of apicoplast division in
466 the absence of TgMyoF. In order to compare parasites at the same stage of cell division, parasites
467 were transiently transfected with a GFP-tubulin expression cassette in order to fluorescently label
468 the pellicle of mother and daughter parasites. Parasites were grown for 12h prior to initiating a 6h

469 treatment with ethanol or 500 μM IAA. Parasites were then stained with anti-Cpn60 antibody and
470 DAPI before image acquisition (Fig. 7A). During elongation, TgMyoF knockdown resulted in a
471 ~25% reduction in apicoplast length (1.54±0.05μm, mean±SEM) when compared to the control
472 parasites (2.11±0.05 μm, mean±SEM) (Fig. 7B). Apicoplast morphology was not disrupted in
473 TgMyoF knockdown parasites in interphase and post-fission stages of division (Fig. S7).

474 **DISCUSSION**

475 The apicoplast is an essential organelle in *T. gondii*. In order to maintain a functional
476 apicoplast, the parasite must execute two distinct yet essential cellular processes: Division of this
477 single copy organelle once per cell cycle to ensure each daughter parasite inherits one apicoplast,
478 and trafficking of nuclear encoded proteins to the apicoplast. We investigated the role of actin
479 and an associated myosin motor, TgMyoF, in these processes. While it had previously been
480 demonstrated that loss of actin and TgMyoF resulted in apicoplast inheritance defects [35], the
481 mechanistic role for these proteins had not been defined. Since we had previously established a
482 role for actin and TgMyoF in dense granule and Rab6 vesicle transport [36,37], determining if
483 this actomyosin system was also involved in apicoplast vesicle trafficking was also warranted.

484 The sequence of events that occur during the apicoplast division cycle had previously been
485 established via fixed cell immunofluorescence of assays or live-cell imaging with low temporal
486 resolution (on the order of minutes) [25,30] (Fig. 1A). This study reveals new insight into how this
487 sequence of events proceeds (Fig. 8). First, the transition from circular to elongated occurs before,
488 and is not dependent on centrosome association, as elongated apicoplasts that are not centrosome
489 associated are frequently observed (Fig. 5 and 6). As a consequence, the elongated apicoplast must

490 orient itself such that each tip of the organelle is associated with a single centrosome. Live cell
491 imaging with high temporal resolution has provided insight into how this is achieved. The
492 centrosome associates with both the sides and tips of the elongated apicoplast. Centrosome sliding
493 along the apicoplast side and branch formation and retraction are likely important for positioning
494 of the centrosome at the apicoplast tips. Consistent with this the localization of TgAtg8 which
495 plays a role in mediating these interactions, is not restricted to the apicoplast tips but found on the
496 entire apicoplast surface (Fig. 6). Loss of TgMyoF results in decreased apicoplast dynamics (Fig.
497 4) and centrosome association (Fig. 6), which ultimately leads to apicoplast inheritance defects.
498 Despite the defects in centrosome-apicoplast association in the absence of TgMyoF, TgAtg8
499 remains localized at the apicoplast. Collectively, this data indicates that actomyosin-driven
500 apicoplast dynamics are important to facilitate the association between these two organelles and
501 for positioning of the centrosomes at the apicoplast tips.

502 While it has long been recognized that apicoplast protein trafficking to the apicoplast is
503 a vital cellular process, our understanding of this trafficking process is incomplete. A number of
504 apicoplast proteins show dual localization to the apicoplast and cytosolic vesicles indicating
505 that vesicular trafficking is one mechanism by which proteins reach the apicoplast. Outstanding
506 questions remained regarding the timing of this trafficking and the proteomic make up of these
507 vesicles. Using TgAPT1 as a marker, this study demonstrates that vesicle trafficking is
508 coordinated with the apicoplast division cycle with the number of vesicles increasing 7-fold
509 during elongation. We hypothesize that the increased trafficking during elongation provides
510 additional lipids and proteins required for increasing apicoplast volume prior to division. The
511 number of vesicles in the cytosol decreases post-fission, as presumably vesicles fuse with the

512 apicoplast.

513 Vesicle trafficking is a multi-step process involving vesicle formation and budding from
514 the donor compartment, transport, docking/tethering to the target membrane and finally vesicle
515 fusion. A 12-hour treatment with CD to induce actin depolymerization and 15-hour treatment
516 with IAA to deplete TgMyoF caused to a significant increase in the number of vesicles in the
517 cytosol at all phases of the cell division cycle. However, we cannot definitively pinpoint which
518 step of the vesicle trafficking pathway is defective in the absence of this actomyosin system.
519 The increased number of vesicles each cell division stage indicates that vesicle formation is not
520 affected, with the caveat that our imaging does not have the temporal or spatial resolution to
521 image individual budding events and so this could not be quantified directly. By tracking the
522 motion of individual vesicles in live parasites we demonstrate that vesicle motion appears
523 predominately diffusive-like. With ~80% of vesicles moving in a random manner, i.e., those
524 with a straightness value less than 0.5 (Fig. 3). "Directed" movements were defined as those
525 with a straightness value greater than 0.5 and a displacement length greater than 500nm. Only
526 ~10% of vesicles in control parasites met these criteria. Actin depolymerization or TgMyoF
527 depletion reduced this percentage by ~50% (Fig. 3). Therefore, we conclude that only a small
528 proportion of vesicles are transported in an actomyosin dependent manner. Given that 90% of
529 vesicles exhibit diffusive motion it is unlikely that the small change in the percentage of
530 vesicles exhibiting directed motor driven movement can account for the large accumulation in
531 vesicles seen after CD and IAA treatment. We interpret the increase in vesicle number at all
532 stages of the cell cycle to be due to vesicles that are formed during elongation but which failed
533 to fuse with the apicoplast. These vesicles remain in the cytosol when the parasites exit the cell

534 cycle and enter interphase. Recent work has shown that the R-SNARE TgVAMP4-2 localizes
535 on the outer membrane of the apicoplast is essential for the trafficking of four luminal and two
536 membrane apicoplast proteins [50]. A full characterization of TgVAMP4-2 and the other
537 components of this SNARE complex (yet to be identified), is required for full understanding of
538 the mechanisms of vesicle fusion with the apicoplast.

539 Consistent with the idea that vesicle fusion is disrupted upon loss of F-actin and
540 TgMyoF, the increased vesicle accumulation was accompanied by decreased apicoplast length
541 during elongation which could result from insufficient delivery of lipids and proteins to the
542 apicoplast prior to division. Despite the shortened length, apicoplast elongation did occur in the
543 absence of F-actin and TgMyoF demonstrating that these proteins are not the main drivers of
544 membrane deformation.

545 TgAPT1 is a membrane associated apicoplast protein and does not contain the canonical
546 signal peptide and apicoplast transit sequence found in other apicoplast proteins, many of which
547 are found in the apicoplast lumen. Luminal proteins TgCpn60 and TgFNR were never observed
548 in TgAPT1 vesicles (Fig. 1; Fig S3 and S4), suggesting that there are two trafficking pathways
549 from the ER to the apicoplasts; one in which proteins are trafficking via vesicles and another
550 where trafficking occurs by an unknown mechanism. It has previously been suggested that ER-
551 apicoplast trafficking could occur via membrane contact sites although the experimental data to
552 support this hypothesis is limited and requires further investigation [51].

553 There are still a number of important outstanding questions that need to be addressed in
554 future studies. How does this actomyosin system interact with the apicoplast in order to drive

555 apicoplast dynamics during elongation? What role do TgMyoF and F-actin play in vesicle
556 docking or fusion with the apicoplast? What proteins drive the dramatic transition from a circular
557 to elongated morphology that occurs at the start of apicoplast division?

558 Overall, our results demonstrate that the actomyosin system comprising actin and TgMyoF
559 play two distinct roles in apicoplast function: Trafficking of ER derived vesicles to the apicoplast
560 and controlling apicoplast dynamics which is needed for apicoplast-centrosome association. This
561 study has refined our understanding of steps in apicoplast division and provides new insights into
562 the mechanisms and timing of protein trafficking to the apicoplast.

563 **ACKNOWLEDGEMENTS**

564 We thank the members of the Heaslip Lab for helpful discussion during the course of these
565 experiments. We thank our colleagues for sharing reagents: Dr. Gary Ward (University of
566 Vermont) for the IMC-1 antibody; Dr. Boris Striepen (University of Pennsylvania) for the anti-
567 Cpn60 antibody. Dr. Ke Hu (Arizona State University) for pTub-mcherry-TubA1 and pTub-
568 eGFP-TubA1, pTub-FNR-RFP plasmids. Dr. Sebastian Besterio (Univ. Montpellier, France) for
569 the pTub-tdTomato-TgAtg8 expression plasmid

570 **FUNDING INFORMATION:**

571 This work was funded by the National Institute of General Medical Sciences 1R35GM138316-01
572 awarded to ATH. The funders had no role in study design, data collection and interpretation, the
573 decision to submit the work for publication or manuscript preparation. The authors declare that
574 no competing interests exist.

575 **REFERENCES**

576 1. Torgerson PR, Mastroiacovo P. The global burden of congenital toxoplasmosis: a
577 systematic review. Bull World Heal Organ. 2013 Jul;91(7):501–8.

578 2. Renaud EA, Pamukcu S, Cerutti A, Berry L, Lemaire-Vieille C, Yamaryo-Botté Y, et al.
579 Disrupting the plastidic iron-sulfur cluster biogenesis pathway in Toxoplasma gondii has
580 pleiotropic effects irreversibly impacting parasite viability. J Biol Chem [Internet]. 2022
581 Aug 1 [cited 2022 Nov 2];298(8). Available from:
582 http://www.jbc.org/article/S0021925822006858/fulltext

583 3. Waller RF, Keeling PJ, Donald RGK, Striepen B, Handman E, Lang-Unnasch N, et al.
584 Nuclear-encoded proteins target to the plastid in Toxoplasma gondii and Plasmodium
585 falciparum. Proc Natl Acad Sci U S A. 1998;95(21):12352–7.

586 4. Yeh E, DeRisi JL. Chemical Rescue of Malaria Parasites Lacking an Apicoplast Defines
587 Organelle Function in Blood-Stage Plasmodium falciparum. PLOS Biol [Internet]. 2011
588 Aug [cited 2022 Nov 2];9(8):e1001138. Available from:
589 https://journals.plos.org/plosbiology/article?id=10.1371/journal.pbio.1001138

590 5. Lim L, McFadden GI. The evolution, metabolism and functions of the apicoplast. Philos
591 Trans R Soc B Biol Sci [Internet]. 2010 Mar 12 [cited 2022 Nov 2];365(1541):749–63.
592 Available from: https://royalsocietypublishing.org/doi/10.1098/rstb.2009.0273

593 6. Bergmann A, Floyd K, Key M, Dameron C, Rees KC, Brock Thornton L, et al.
594 Toxoplasma gondii requires its plant-like heme biosynthesis pathway for infection. PLOS

595 Pathog [Internet]. 2020 May 1 [cited 2022 Nov 2];16(5):e1008499. Available from:
596 https://journals.plos.org/plospathogens/article?id=10.1371/journal.ppat.1008499

597 7. Sheiner L, Vaidya AB, McFadden GI. The metabolic roles of the endosymbiotic
598 organelles of Toxoplasma and Plasmodium spp. Curr Opin Microbiol. 2013 Aug
599 1;16(4):452–8.

600 8. Brooks CF, Johnsen H, van Dooren GG, Muthalagi M, Lin SS, Bohne W, et al. The
601 Toxoplasma Apicoplast Phosphate Translocator Links Cytosolic and Apicoplast
602 Metabolism and Is Essential for Parasite Survival. Cell Host Microbe [Internet]. 2010 Jan
603 21 [cited 2022 Nov 2];7(1):62–73. Available from:
604 http://www.cell.com/article/S1931312809004120/fulltext

605 9. Fichera ME, Roos DS. A plastid organelle as a drug target in apicomplexan parasites.
606 Nature. 1997;390(6658):407–9.

607 10. He CY, Shaw MK, Pletcher CH, Striepen B, Tilney LG, Roos DS. A plastid segregation
608 defect in the protozoan parasite Toxoplasma gondii. EMBO J. 2001;20(3):330–9.

609 11. Pfefferkorn ER, Nothnagel RF, Borotz SE. Parasiticidal effect of clindamycin on
610 Toxoplasma gondii grown in cultured cells and selection of a drug-resistant mutant.
611 Antimicrob Agents Chemother [Internet]. 1992 [cited 2022 Nov 2];36(5):1091–6.
612 Available from: https://journals.asm.org/doi/10.1128/AAC.36.5.1091

613 12. Harb OS, Chatterjee B, Fraunholz MJ, Crawford MJ, Nishi M, Roos DS. Multiple
614 functionally redundant signals mediate targeting to the apicoplast in the apicomplexan

615 parasite Toxoplasma gondii. Eukaryot Cell [Internet]. 2004 Jun [cited 2022 Nov
616 2];3(3):663–74. Available from: https://journals.asm.org/doi/10.1128/EC.3.3.663-
617 674.2004

618 13. DeRocher A, Hagen CB, Froehlich JE, Feagin JE, Parsons M. Analysis of targeting
619 sequences demonstrates that trafficking to the Toxoplasma gondii plastid branches off the
620 secretory system. J Cell Sci [Internet]. 2000 Nov 15 [cited 2022 Nov 2];113(22):3969–77.
621 Available from: https://journals.biologists.com/jcs/article/113/22/3969/26332/Analysis-of-
622 targeting-sequences-demonstrates-that

623 14. Parsons M, Karnataki A, Feagin JE, DeRocher A. Protein trafficking to the apicoplast:
624 deciphering the apicomplexan solution to secondary endosymbiosis. Eukaryot Cell
625 [Internet]. 2007 Jul [cited 2022 Dec 14];6(7):1081–8. Available from:
626 https://pubmed.ncbi.nlm.nih.gov/17513565/

627 15. Derocher AE, Karnataki A, Vaney P, Parsons M. Apicoplast Targeting of a Toxoplasma
628 gondii Transmembrane Protein Requires a Cytosolic Tyrosine-Based Motif. Traffic.
629 2012;13(5):694–704.

630 16. DeRocher AE, Coppens I, Karnataki A, Gilbert LA, Rome ME, Feagin JE, et al. A
631 thioredoxin family protein of the apicoplast periphery identifies abundant candidate
632 transport vesicles in Toxoplasma gondii. Eukaryot Cell [Internet]. 2008;7(9):1518–29.
633 Available from: http://www.ncbi.nlm.nih.gov/pubmed/18586952

634 17. Karnataki A, Derocher AE, Coppens I, Feagin JE, Parsons M. A Membrane Protease is

635 Targeted to the Relict Plastid of Toxoplasma via an Internal Signal Sequence. Traffic
636 [Internet]. 2007 Nov 1 [cited 2022 Nov 4];8(11):1543–53. Available from:
637 https://onlinelibrary.wiley.com/doi/full/10.1111/j.1600-0854.2007.00637.x

638 18. Karnataki A, DeRocher AE, Feagin JE, Parsons M. Sequential processing of the
639 Toxoplasma apicoplast membrane protein FtsH1 in topologically distinct domains during
640 intracellular trafficking. Mol Biochem Parasitol. 2009 Aug 1;166(2):126–33.

641 19. McFadden GI, Yeh E. The apicoplast: now you see it, now you don't. Int J Parasitol
642 [Internet]. 2017 Feb 1 [cited 2022 Dec 14];47(2–3):137–44. Available from:
643 https://pubmed.ncbi.nlm.nih.gov/27773518/

644 20. Van Dooren GG, Tomova C, Agrawal S, Humbel BM, Striepen B. Toxoplasma gondii
645 Tic20 is essential for apicoplast protein import. Proc Natl Acad Sci U S A [Internet]. 2008
646 Sep 9 [cited 2022 Dec 14];105(36):13574–9. Available from:
647 https://pubmed.ncbi.nlm.nih.gov/18757752/

648 21. Sheiner L, Fellows JD, Ovciarikova J, Brooks CF, Agrawal S, Holmes ZC, et al.
649 Toxoplasma gondii Toc75 Functions in Import of Stromal but not Peripheral Apicoplast
650 Proteins. Traffic [Internet]. 2015 Dec 1 [cited 2022 Dec 14];16(12):1254–69. Available
651 from: https://pubmed.ncbi.nlm.nih.gov/26381927/

652 22. Felsner G, Sommer MS, Gruenheit N, Hempel F, Moog D, Zauner S, et al. ERAD
653 components in organisms with complex red plastids suggest recruitment of a preexisting
654 protein transport pathway for the periplastid membrane. Genome Biol Evol [Internet].

655 2011 [cited 2022 Dec 14];3(1):140–50. Available from:
656 https://pubmed.ncbi.nlm.nih.gov/21081314/

657 23. Sommer MS, Gould SB, Lehmann P, Gruber A, Przyborski JM, Maier UG. Der1-
658 mediated preprotein import into the periplastid compartment of chromalveolates? Mol
659 Biol Evol [Internet]. 2007 Apr [cited 2022 Dec 14];24(4):918–28. Available from:
660 https://pubmed.ncbi.nlm.nih.gov/17244602/

661 24. Mallo N, Fellows J, Johnson C, Sheiner L. Protein Import into the Endosymbiotic
662 Organelles of Apicomplexan Parasites. Genes (Basel) [Internet]. 2018 Aug 14 [cited 2022
663 Dec 14];9(8). Available from: https://pubmed.ncbi.nlm.nih.gov/30110980/

664 25. Striepen B, Crawford MJ, Shaw MK, Tilney LG, Seeber F, Roos DS. The plastid of
665 Toxoplasma gondii is divided by association with the centrosomes. J Cell Biol.
666 2000;151(7):1423–34.

667 26. Lévêque MF, Berry L, Cipriano MJ, Nguyen HM, Striepen B, Besteiro S. Autophagy-
668 related protein ATG8 has a noncanonical function for apicoplast inheritance in
669 toxoplasma gondii. MBio [Internet]. 2015 Oct 27 [cited 2022 Nov 4];6(6). Available
670 from: https://journals.asm.org/doi/10.1128/mBio.01446-15

671 27. Cheng L, Tian Y, Wang Y, Wang T, Yao Y, Yu H, et al. Toxoplasma TgAtg8-TgAtg3
672 Interaction Primarily Contributes to Apicoplast Inheritance and Parasite Growth in
673 Tachyzoite . Microbiol Spectr [Internet]. 2022 Feb 23 [cited 2022 Nov 4];10(1). Available
674 from: https://journals.asm.org/doi/10.1128/spectrum.01495-21

675 28. Mizushima N, Sahani MH. ATG8 localization in apicomplexan parasites.
676 http://dx.doi.org/104161/auto32183 [Internet]. 2014 Sep 1 [cited 2022 Nov
677 4];10(9):1487–94. Available from:
678 https://www.tandfonline.com/doi/abs/10.4161/auto.32183

679 29. Walczak M, Ganesan SM, Niles JC, Yeh E. ATG8 Is Essential Specifically for an
680 Autophagy-Independent Function in Apicoplast Biogenesis in Blood-Stage Malaria
681 Parasites. MBio [Internet]. 2018 Jan 1 [cited 2022 Nov 4];9(1). Available from:
682 https://pubmed.ncbi.nlm.nih.gov/29295911/

683 30. Nishi M, Hu K, Murray JM, Roos DS. Organellar dynamics during the cell cycle of
684 Toxoplasma gondii. J Cell Sci [Internet]. 2008;121(Pt 9):1559–68. Available from:
685 https://www.ncbi.nlm.nih.gov/pubmed/18411248

686 31. Francia ME, Striepen B. Cell division in apicomplexan parasites. Nat Rev Microbiol
687 [Internet]. 2014;12(2):125–36. Available from: http://dx.doi.org/10.1038/nrmicro3184

688 32. van Dooren GG, Reiff SB, Tomova C, Meissner M, Humbel BM, Striepen B. A novel
689 dynamin-related protein has been recruited for apicoplast fission in Toxoplasma gondii.
690 Curr Biol [Internet]. 2009;19(4):267–76. Available from:
691 https://www.ncbi.nlm.nih.gov/pubmed/19217294

692 33. Tosetti N, Pacheco NDS, Favre DS, Jacot D. Three f-actin assembly centers regulate
693 organelle inheritance, cell-cell communication and motility in toxoplasma gondii. Elife.
694 2019 Feb 1;8.

695 34. Stortz JF, Del Rosario M, Singer M, Wilkes JM, Meissner M, Das S. Formin-2 drives
696 polymerisation of actin filaments enabling segregation of apicoplasts and cytokinesis in
697 Plasmodium falciparum. Elife. 2019;

698 35. Jacot D, Daher W, Soldati-Favre D. Toxoplasma gondii myosin F, an essential motor for
699 centrosomes positioning and apicoplast inheritance. EMBO J [Internet]. 2013/05/23. 2013;
700 Available from: http://www.ncbi.nlm.nih.gov/pubmed/23695356

701 36. Heaslip AT, Nelson SR, Warshaw DM. Dense granule trafficking in Toxoplasma gondii
702 requires a unique class 27 myosin and actin filaments. Mol Biol Cell [Internet].
703 2016;27(13):2080–9. Available from: https://www.ncbi.nlm.nih.gov/pubmed/27146112

704 37. Carmeille R, Lomoriello PS, Devarakonda PM, Kellermeier JA, Heaslip AT. Actin and an
705 unconventional myosin motor, TgMyoF, control the organization and dynamics of the
706 endomembrane network in Toxoplasma gondii [Internet]. Vol. 17, PLoS Pathogens. 2021.
707 1–32 p. Available from: http://dx.doi.org/10.1371/journal.ppat.1008787

708 38. Brown K, Long S, Sibley L. Conditional Knockdown of Proteins Using Auxin-inducible
709 Degron (AID) Fusions in Toxoplasma gondii. BIO-PROTOCOL. 2018;

710 39. Brown KM, Long S, Sibley LD. Plasma membrane association by N-acylation governs
711 PKG function in Toxoplasma gondii. MBio. 2017;

712 40. Roos DS, Donald RG, Morrissette NS, Moulton AL. Molecular tools for genetic
713 dissection of the protozoan parasite Toxoplasma gondii. Methods Cell Biol [Internet].
714 1994;45:27–63. Available from: http://www.ncbi.nlm.nih.gov/pubmed/7707991

715 41. Fox BA, Ristuccia JG, Gigley JP, Bzik DJ. Efficient gene replacements in Toxoplasma
716 gondii strains deficient for nonhomologous end joining. Eukaryot Cell [Internet]. 2009
717 Apr [cited 2022 Nov 4];8(4):520–9. Available from:
718 https://journals.asm.org/doi/10.1128/EC.00357-08

719 42. Huynh MH, Carruthers VB. Tagging of endogenous genes in a Toxoplasma gondii strain
720 lacking Ku80. Eukaryot Cell [Internet]. 2009 Apr [cited 2022 Nov 4];8(4):530–9.
721 Available from: https://journals.asm.org/doi/10.1128/EC.00358-08

722 43. Shen B, Brown KM, Lee TD, David Sibley L. Efficient gene disruption in diverse strains
723 of Toxoplasma gondii using CRISPR/CAS9. MBio [Internet]. 2014 May 13 [cited 2022
724 Dec 14];5(3). Available from: https://pubmed.ncbi.nlm.nih.gov/24825012/

725 44. Donald RGK, Roos DS. Insertional mutagenesis and marker rescue in a protozoan
726 parasite: cloning of the uracil phosphoribosyltransferase locus from Toxoplasma gondii.
727 Proc Natl Acad Sci U S A [Internet]. 1995 Jun 6 [cited 2022 Dec 14];92(12):5749–53.
728 Available from: https://pubmed.ncbi.nlm.nih.gov/7777580/

729 45. Lord SJ, Velle KB, Mullins RD, Fritz-Laylin LK. SuperPlots: Communicating
730 reproducibility and variability in cell biology. J Cell Biol. 2020;

731 46. Bouchut A, Geiger JA, Derocher AE, Parsons M. Vesicles bearing Toxoplasma apicoplast
732 membrane proteins persist following loss of the relict plastid or Golgi body disruption.
733 PLoS One [Internet]. 2014 Nov 1 [cited 2022 Dec 14];9(11). Available from:
734 https://pubmed.ncbi.nlm.nih.gov/25369183/

735 47. Hartmann J, Hu K, He CY, Pelletier L, Roos DS, Warren G. Golgi and centrosome cycles
736 in Toxoplasma gondii. Mol Biochem Parasitol. 2006 Jan;145(1):125–7.

737 48. Suvorova ES, Francia M, Striepen B, White MW. A Novel Bipartite Centrosome
738 Coordinates the Apicomplexan Cell Cycle. PLOS Biol [Internet]. 2015 Mar 3 [cited 2022
739 Nov 4];13(3):e1002093. Available from:
740 https://journals.plos.org/plosbiology/article?id=10.1371/journal.pbio.1002093

741 49. Hu K. Organizational changes of the daughter basal complex during the parasite
742 replication of Toxoplasma gondii. PLoS Pathog. 2008;4(1):0108–21.

743 50. Cao S, Yang J, Fu J, Chen H, Jia H. The dissection of SNAREs reveals key factors for
744 vesicular trafficking to the endosome-like compartment and apicoplast via the secretory
745 system in toxoplasma gondii. MBio [Internet]. 2021 Aug 1 [cited 2022 Nov 4];12(4).
746 Available from: https://journals.asm.org/doi/10.1128/mBio.01380-21

747 51. Vaishnava S, Morrison DP, Gaji RY, Murray JM, Entzeroth R, Howe DK, et al. Plastid
748 segregation and cell division in the apicomplexan parasite Sarcocystis neurona. J Cell Sci
749 [Internet]. 2005 Aug 1 [cited 2022 Nov 4];118(15):3397–407. Available from:
750 https://journals.biologists.com/jcs/article/118/15/3397/28470/Plastid-segregation-and-cell-
751 division-in-the

752

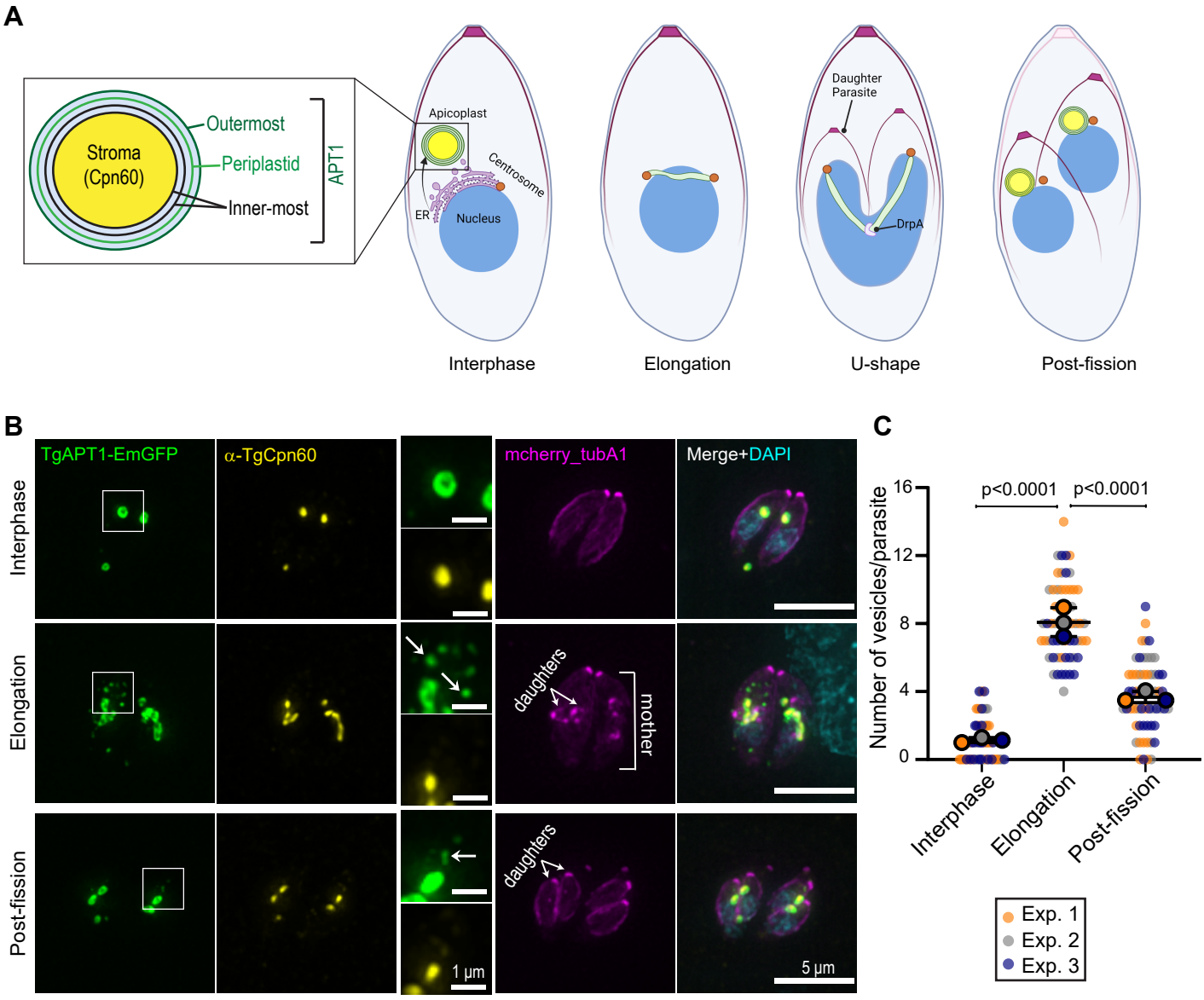
A
Stroma
(Cpn60)
Outermost
Periplastid
Inner-most
APT1
Apicoplast
Centrosome
ER
Nucleus
Daughter
Parasite
DrpA
Interphase
Elongation
U-shape
Post-fission
B
TgAPT1-EmGFP
α-TgCpn60
mcherry_tubA1
Merge+DAPI
Interphase
Elongation
Post-fission
daughters
mother
daughters
1 µm
5 µm
C
Number of vesicles/parasite
16
12
8
4
0
p<0.0001
p<0.0001
Interphase
Elongation
Post-fission
Exp. 1
Exp. 2
Exp. 3

Figure 1

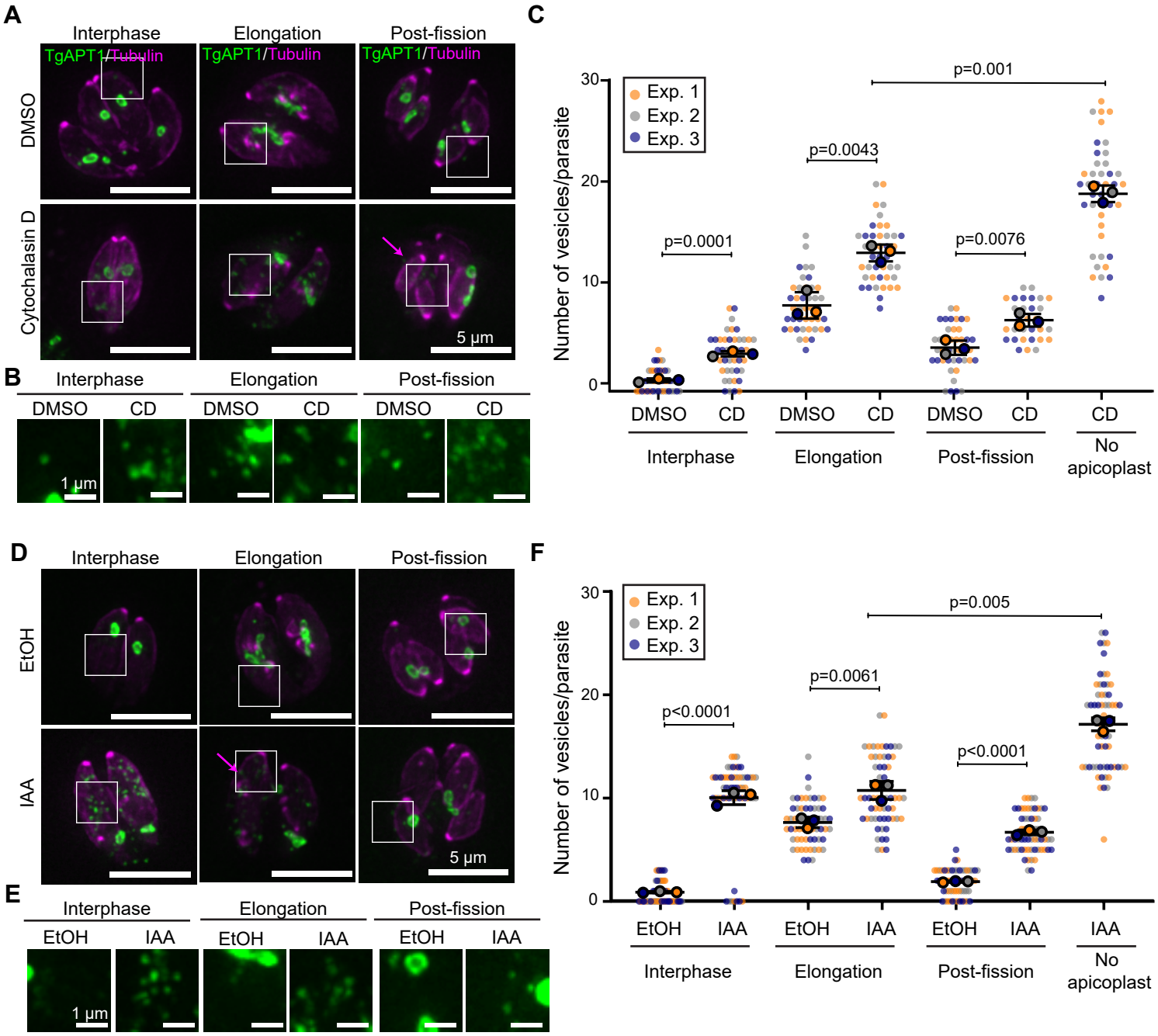
A
Interphase
Elongation
Post-fission
TgAPT1/Tubulin
DMSO
Cytochalasin D
5 µm
B
Interphase
Elongation
Post-fission
DMSO
CD
1 µm
C
Exp. 1
Exp. 2
Exp. 3
Number of vesicles/parasite
p=0.0001
p=0.0043
p=0.0076
p=0.001
Interphase
Elongation
Post-fission
No apicoplast
D
EtOH
IAA
E
F
p<0.0001
p=0.0061
p<0.0001
p=0.005

Figure 2.

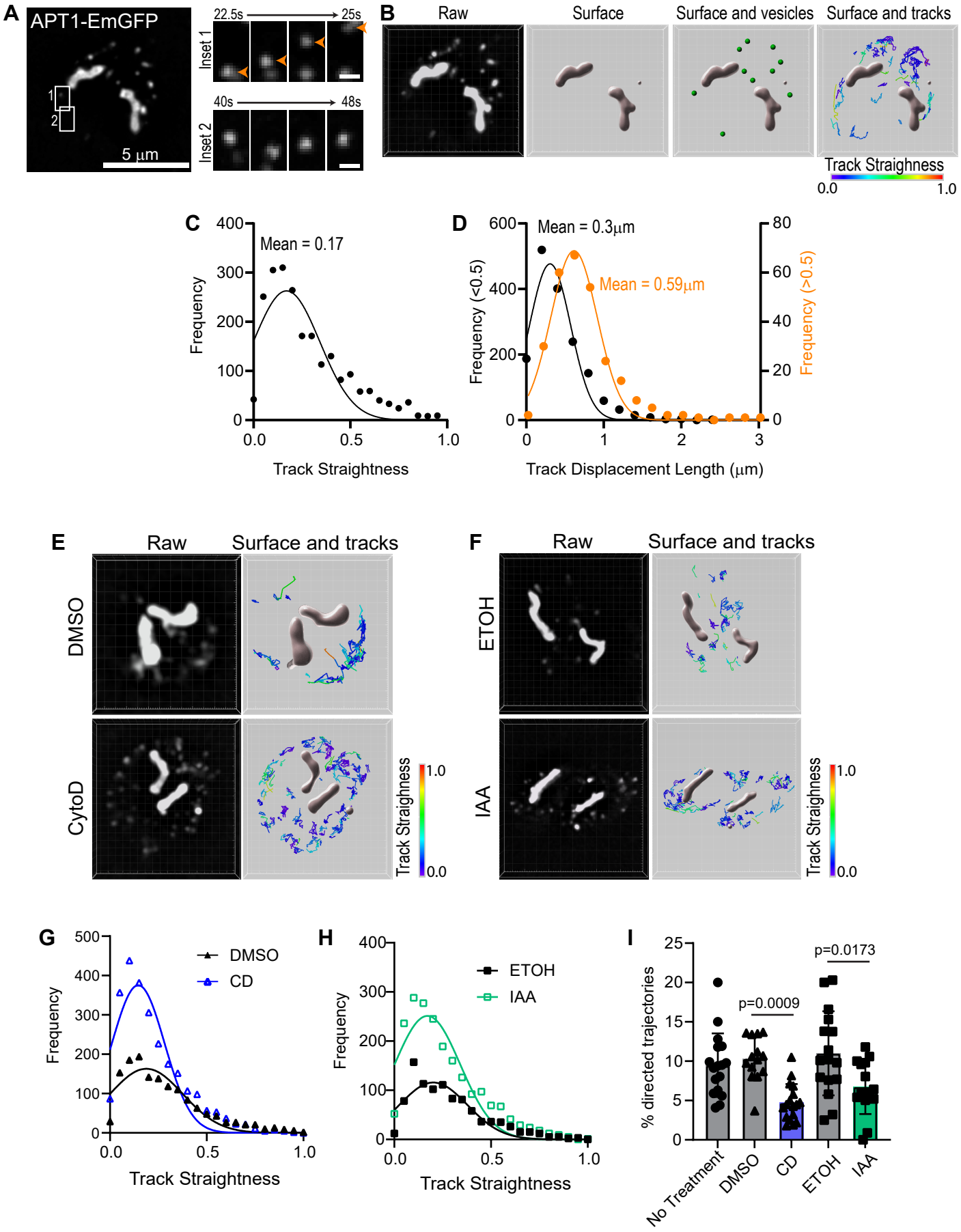
A
APT1-EmGFP
1
2
5 µm
22.5s
25s
Inset 1
40s
48s
Inset 2
B
Raw
Surface
Surface and vesicles
Surface and tracks
Track Straighness
0.0
1.0
C
Mean = 0.17
Frequency
Track Straightness
D
Mean = 0.3µm
Mean = 0.59µm
Frequency (<0.5)
Frequency (>0.5)
Track Displacement Length (µm)
E
Raw
Surface and tracks
DMSO
CytoD
Track Straighness
F
Raw
Surface and tracks
ETOH
IAA
Track Straighness
G
DMSO
CD
Frequency
Track Straightness
H
ETOH
IAA
Frequency
Track Straightness
I
p=0.0009
p=0.0173
% directed trajectories
No Treatment
DMSO
CD
ETOH
IAA

Figure 3.

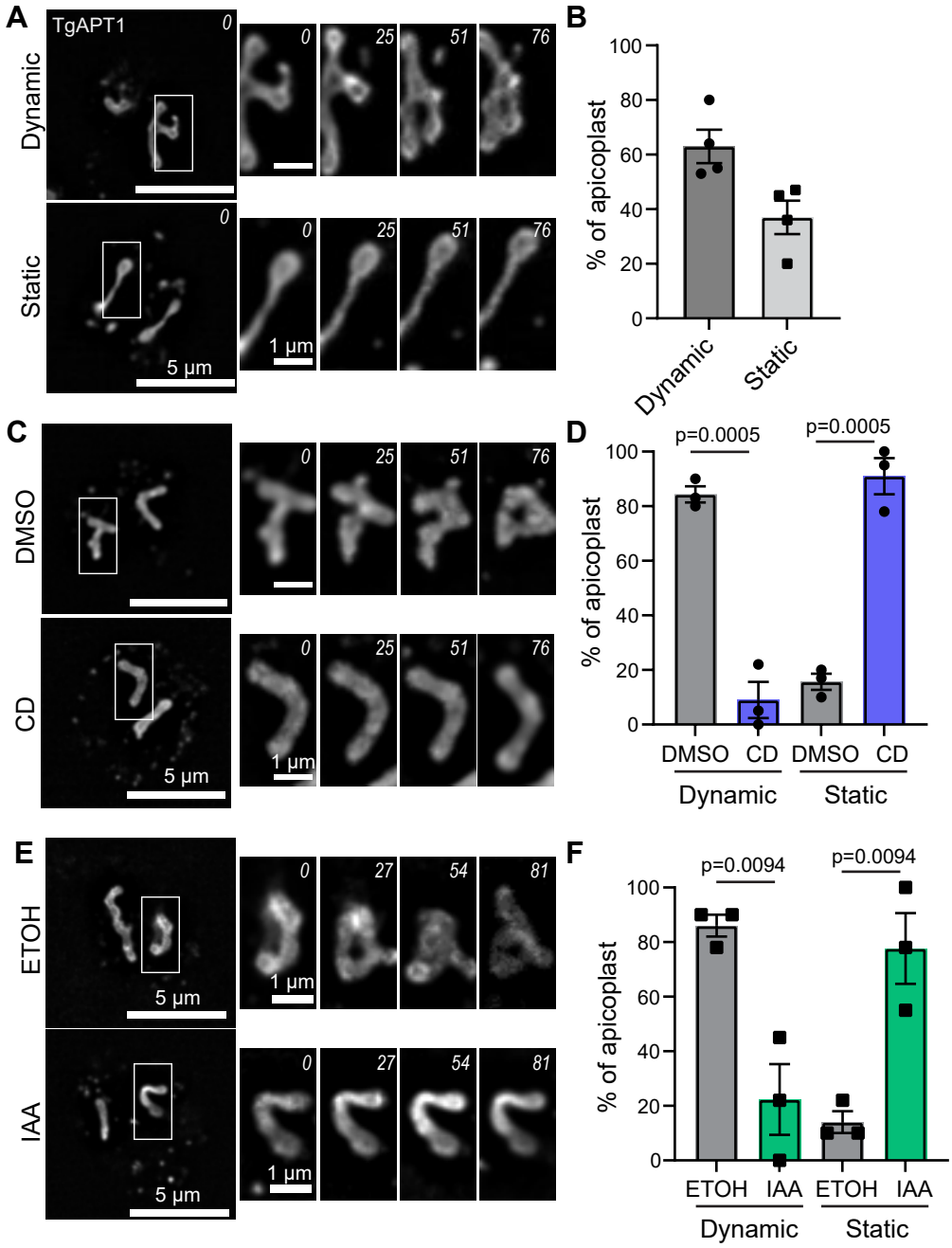
A
TgAPT1
Dynamic
Static
0
25
51
76
5 µm
1 µm
B
% of apicoplast
Dynamic
Static
C
DMSO
CD
D
p=0.0005
p=0.0005
DMSO
CD
Dynamic
Static
E
ETOH
IAA
27
54
81
F
p=0.0094
p=0.0094
ETOH
IAA

Figure 4.

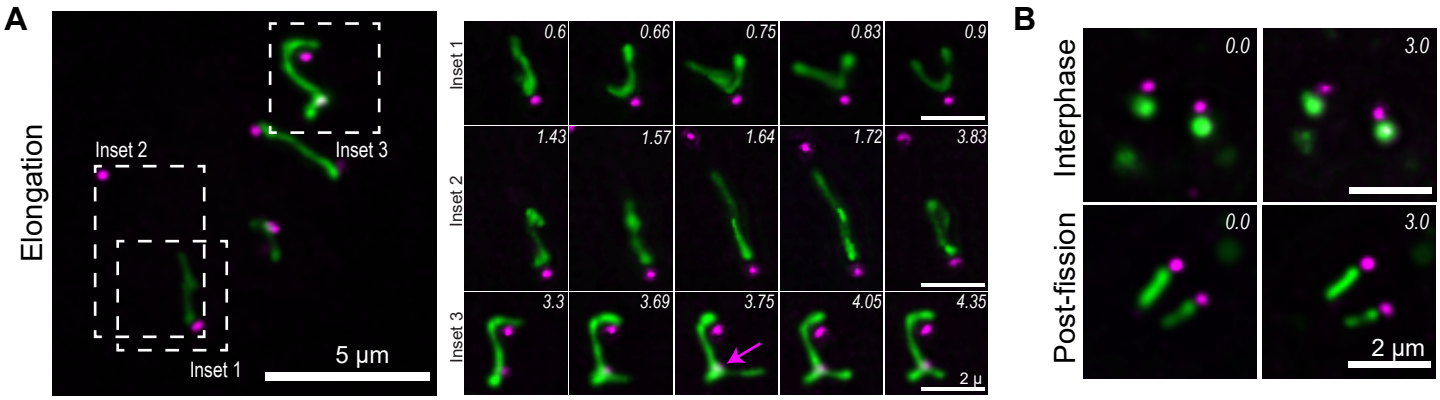
A
Elongation
Inset 2
Inset 3
Inset 1
5 µm
Inset 1
0.6
0.66
0.75
0.83
0.9
Inset 2
1.43
1.57
1.64
1.72
3.83
Inset 3
3.3
3.69
3.75
4.05
4.35
2 µ
B
Interphase
0.0
3.0
Post-fission
0.0
3.0
2 µm

Figure 5.

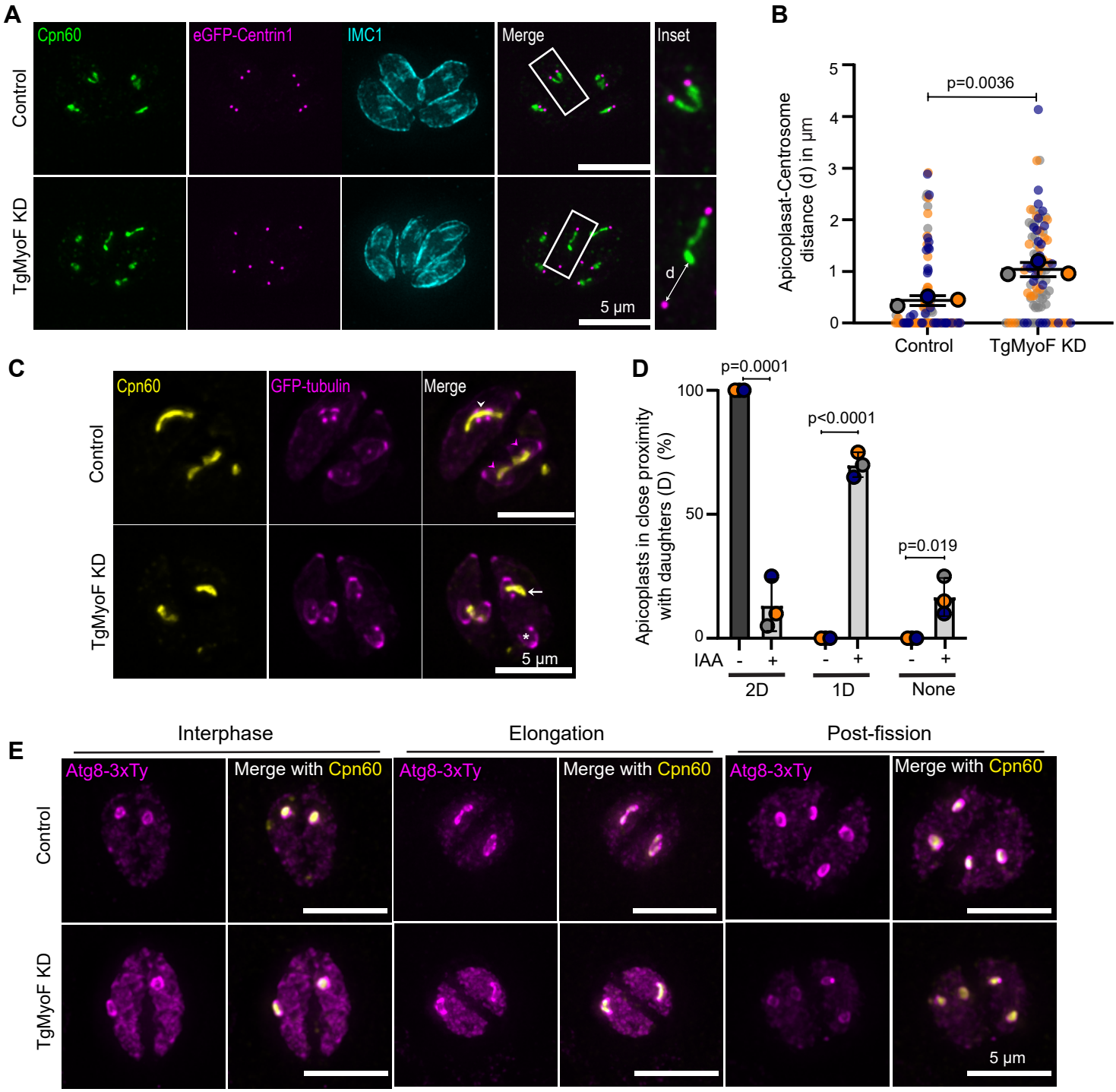
A
Cpn60
eGFP-Centrin1
IMC1
Merge
Inset
Control
TgMyoF KD
d
5 µm
B
Apicoplasat-Centrosome distance (d) in µm
p=0.0036
Control
TgMyoF KD
C
Cpn60
GFP-tubulin
Merge
Control
TgMyoF KD
5 µm
D
Apicoplasts in close proximity with daughters (D) (%)
p=0.0001
p<0.0001
p=0.019
IAA
2D
1D
None
E
Interphase
Elongation
Post-fission
Atg8-3xTy
Merge with Cpn60
Control
TgMyoF KD
5 µm

Figure 6.

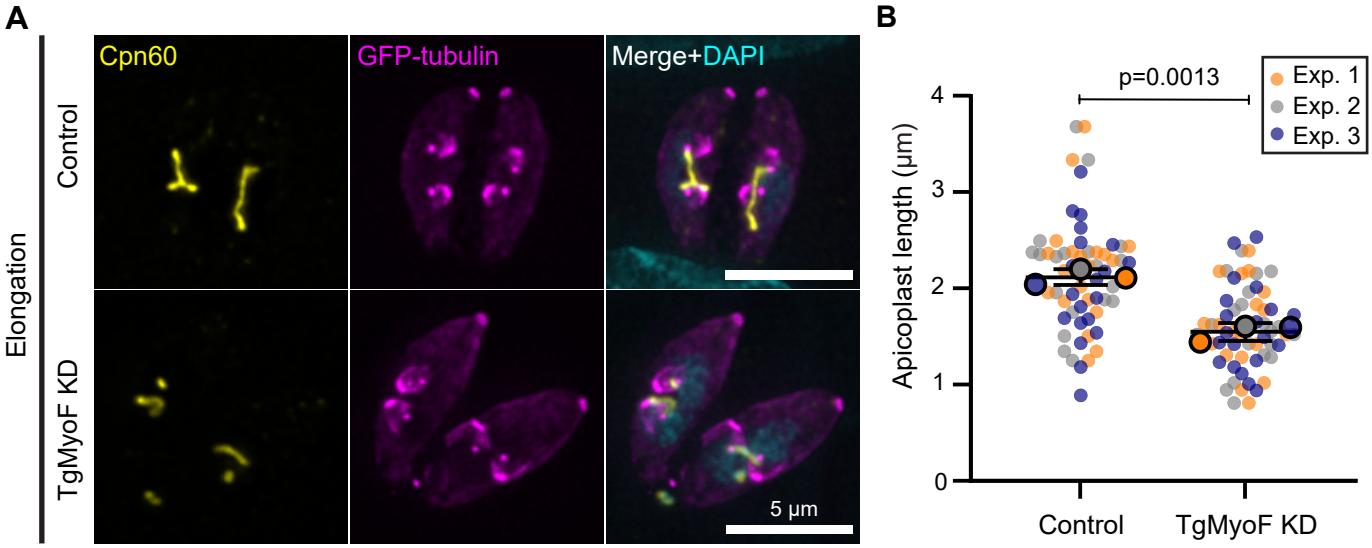
A
Elongation
Control
TgMyoF KD
Cpn60
GFP-tubulin
Merge+DAPI
5 µm
B
p=0.0013
Exp. 1
Exp. 2
Exp. 3
Apicoplast length (µm)
0
1
2
3
4
Control
TgMyoF KD

Figure 7.

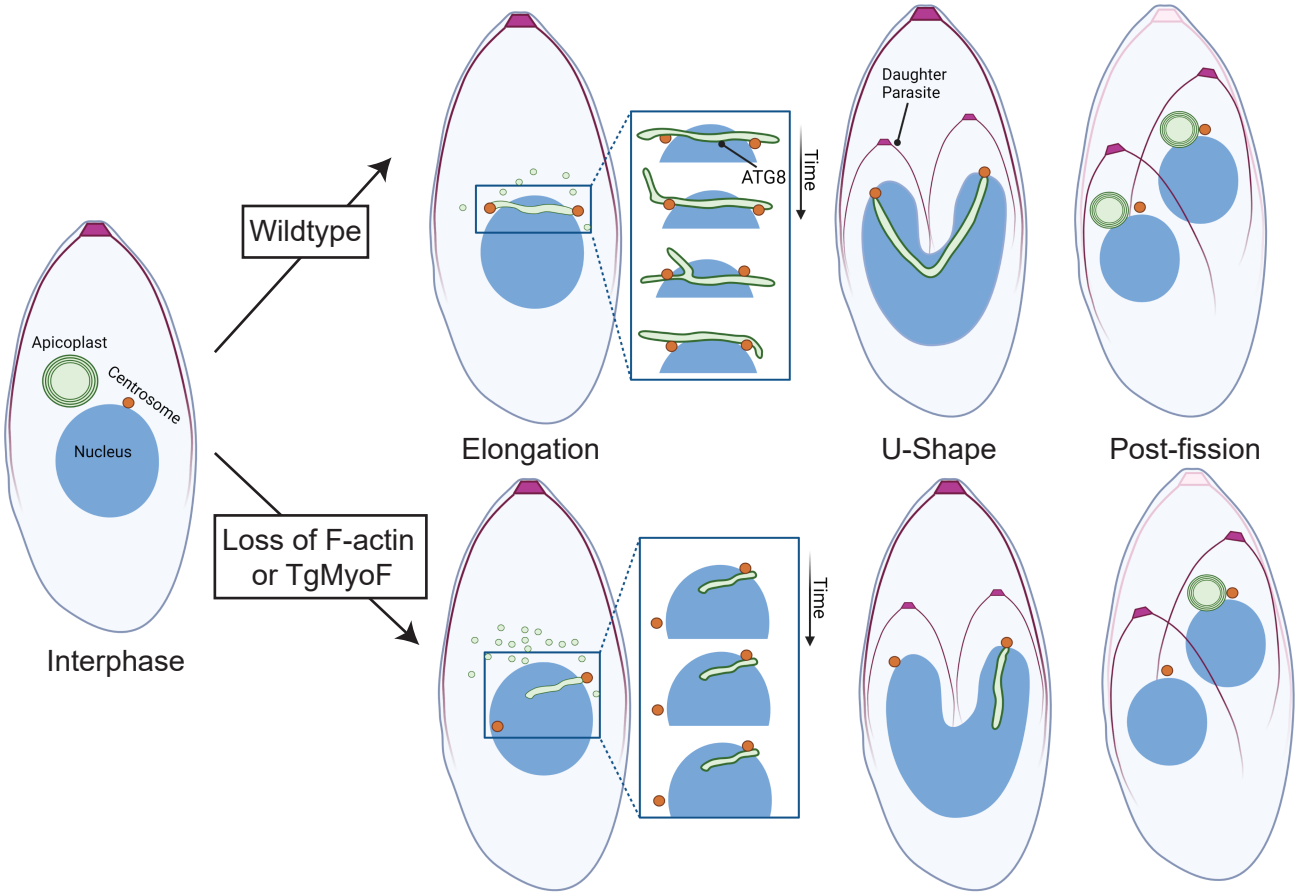
Apicoplast
Centrosome
Nucleus
Interphase
Wildtype
Loss of F-actin
or TgMyoF
ATG8
Time
Elongation
Daughter
Parasite
U-Shape
Post-fission
Time

Figure 8.

Supplementary figures

Trafficking of nuclear-encoded apicoplast proteins depends on F-actin and Myosin F in *Toxoplasma gondii*

Devarakonda et al.,

Figure S1: Creation of TgAPT1-EmGFP parasite line

(A) Schematic of TgAPT1 genomic locus in parental Ku80 parasites and TgAPT1-EmGFP knock-in parasites. Binding sites of primers used for diagnostic PCR are indicated. Expected PCR product size with F1 and R1 primers is 1785bp. Expected PCR product size for F1 and R2 primers is 1053bp. (B) Diagnostic PCR with F1/R2 and F1/R1 primer pairs using genomic DNA from parental Ku80 and APT1 knock-in parasites as a template.

Figure S2: Creation of TgMyoF-AID: TgAPT1-EmGFP parasite line

(A) Schematic of UPRT genomic locus in parental TgMyoF-AID parasites and TgMyoF-AID:TgAPT1-EmGFP knock-in parasites. Binding sites of proteins used for diagnostic PCR are indicated. Expected PCR product size with F1 and R1 primers is 1101bp. Expected PCR product size for F1 and R2 primers is 2373bp. (B) Diagnostic PCR with F1/R1 and F1/R2 primer pairs using genomic DNA from parental and knock-in parasites as a template.

Figure S3: Actin depolymerization with cytochalasin D causes an accumulation of TgAPT1 vesicles in the cytosol

Fluorescent images of TgAPT1-EmGFP parasites treated with DMSO (control) or 0.2 μM cytochalasin D treated for 12 hours that were categorized as interphase, elongation and post-fission stages of the apicoplast division cycle. Parasites were fixed and stained with anti-Cpn60 antibody (a marker for the apicoplast shown in yellow) and DAPI (cyan). Panels are maximum intensity projections of deconvolved images. Scale bar represents 5 μm. White box indicates area used to make inset. Inset: Brightness and contrast of insets was adjusted to facilitate visualization of dimmer TgAPT1 vesicles. Inset scale bar represents 2 μm.

Figure S4: TgMyoF knockdown causes an accumulation of TgAPT1 vesicles in the cytosol

Fluorescent images of TgMyoF-mAID; TgAPT1-EmGFP parasites treated with ethanol (control) or 500 μM IAA treated for 15 hours and then categorized as being in the interphase, elongation and post-fission stages of the apicoplast division cycle. Parasites were fixed and stained with anti-Cpn60 antibody (a marker for the apicoplast shown in yellow) and DAPI (cyan). Panels are maximum intensity projections of deconvolved images. Scale bar represents 5 μm. White box indicates area used to make inset. Inset: Brightness and contrast of insets was adjusted to facilitate visualization of dimmer TgAPT1 vesicles. Inset scale bar represents 2 μm.

Figure S5: TgMyoF knockdown results in asymmetric localization of elongated apicoplast to daughter parasites.

Maximum intensity projection of deconvolved fluorescent images of TgMyoF-AID parasites treated with ethanol or IAA. Parasites are expressing eGFP-tubulin (magenta) stained with anti-Cpn60 antibody (yellow). Control parasites show that the elongated apicoplasts are in proximity to the daughter parasites (white arrowheads). Later in division, the tips of the elongated apicoplast are localized with the growing daughters (magenta arrowheads). Upon TgMyoF KD, there is an asymmetric localization of the elongated apicoplast to one of the daughter cells (white arrow). Parasites where the apicoplast association with the daughters appears normal is indicates with a white arrowhead. In some parasites the apicoplast is not associated with either daughter (indicated with an asterisk). Scale bar represents 5 μm.

Figure S6: TgMyoF knockdown does not disrupt ATG8 association with the apicoplast.

TgMyoF-mAID parasites ectopically expressing 3xTy-Atg8 under the Atg8 promoter were grown for 12 hours before treatment with ethanol (control) or IAA (TgMyoF KD) for 6 hours. Cell were stained with anti-Ty (magenta) and anti-Cpn60 antibodies (yellow), and DAPI.

Maximum intensity projections of deconvolved images of parasites during interphase, elongation and post-fission are shown. Scale bar represents 5 µm

Figure S7: TgMyoF knockdown did not lead to changes in apicoplats morphology in interphase of post-fission stages of apicoplast division.

(A) TgMyoF-mAID parasites expressing eGFP-tubulin (magenta) grown for 12 hours before treatment with ethanol (control) or IAA (TgMyoF KD) for 6 hours. Parasites with an anti-Cpn60 antibody (yellow) and DAPI (cyan). Parasites in interphase and post-fission stages of apicopalst divison are shown. Scale bar represents 5 µm.

Table S1: List of plasmids used in this study

Table S2: List of primers used in this study

Table S3: List of gene accession numbers associated with this study

Table S4: List of antibodies used in this study

Video S1: TgAPT1-EmGFP parasites were imaged in the elongation phase of apicoplast division. Images are maximum intensity projection of deconvolved images that contained 3 Z-slices with 0.4µm step size between planes. Imaging speed/stack was 2 stacks/second. Playback speed is 30fps or 15x real time.

Video S2: TgAPT1-EmGFP parasites were imaged in the elongation phase of apicoplast division. Examples of apicoplast that are dynamic (left) and static (right) over the imaging period. Images are maximum intensity projection of deconvolved images that contained 3 Z-

slices with 0.4µm step size between planes. Imaging speed/stack was 2 stacks/second. Playback speed is 40fps or 20x real time.

Video S3: TgAPT1-EmGFP parasites treated with DMSO (left) and CD (right) for 30 minutes were imaged in the elongation phase of apicoplast division. Images are maximum intensity projection of deconvolved images that contained 3 Z-slices with 0.4µm step size between planes. Imaging speed/stack was 2 stacks/second. Playback speed is 30fps or 15x real time.

Video S4: TgMyoF-AID: TgAPT1-EmGFP parasites treated with ethanol (left) or IAA (right) for 15 hours were imaged in the elongation phase of apicoplast division. Images are maximum intensity projection of deconvolved images that contained 3 Z-slices with 0.4µm step size between planes. Imaging speed/stack was 0.5 stacks/second. Playback speed is 25fps or 12x real time.

Video S5: RH parasites expressing and pmin-Centrin1-eGFP (centrosome marker; magenta) ptub-FNR-RFP (apicoplast marker; green) in the elongation phase of apicoplast division. Images are maximum intensity projection of deconvolved images that contained 5 Z-slices with 0.4um step size between planes. Images were acquired channel 1/channel 2 at each Z slice. Time lag between channels was ~0.4 seconds. Imaging speed is 4.6s/2-color stack. Total imaging time is 9 minutes. Playback speed is 20fps or 84x real time. Raw data was bleach and drift corrected as outlined in materials and methods

Video S6: Inset 1 from Video S8/Figure 5. Playback speed is 5fps or 22x real time.

Video S7: Inset 2 from Video S8/Figure 5. Playback speed is 10fps or 45x real time.

Video S8: Inset 3 from Video S8/Figure 5. Playback speed is 10fps or 22x real time.

Video S09: RH parasites expressing and pmin-Centrin1-eGFP (centrosome marker; magenta) ptub-FNR-RFP (apicoplast marker; green) in interphase and post-fission. Images are maximum intensity projections of deconvolved images that contained 5 Z-slices with 0.4μm step size between planes. Images were acquired channel 1/channel 2 at each Z slice. Time lag between channels was ~0.4 seconds. Imaging speed is 7.8s/2-color stack. Total imaging time is 2.5 minutes. Playback speed is 60x real time. Raw data was bleach and drift corrected as outlined in materials and methods

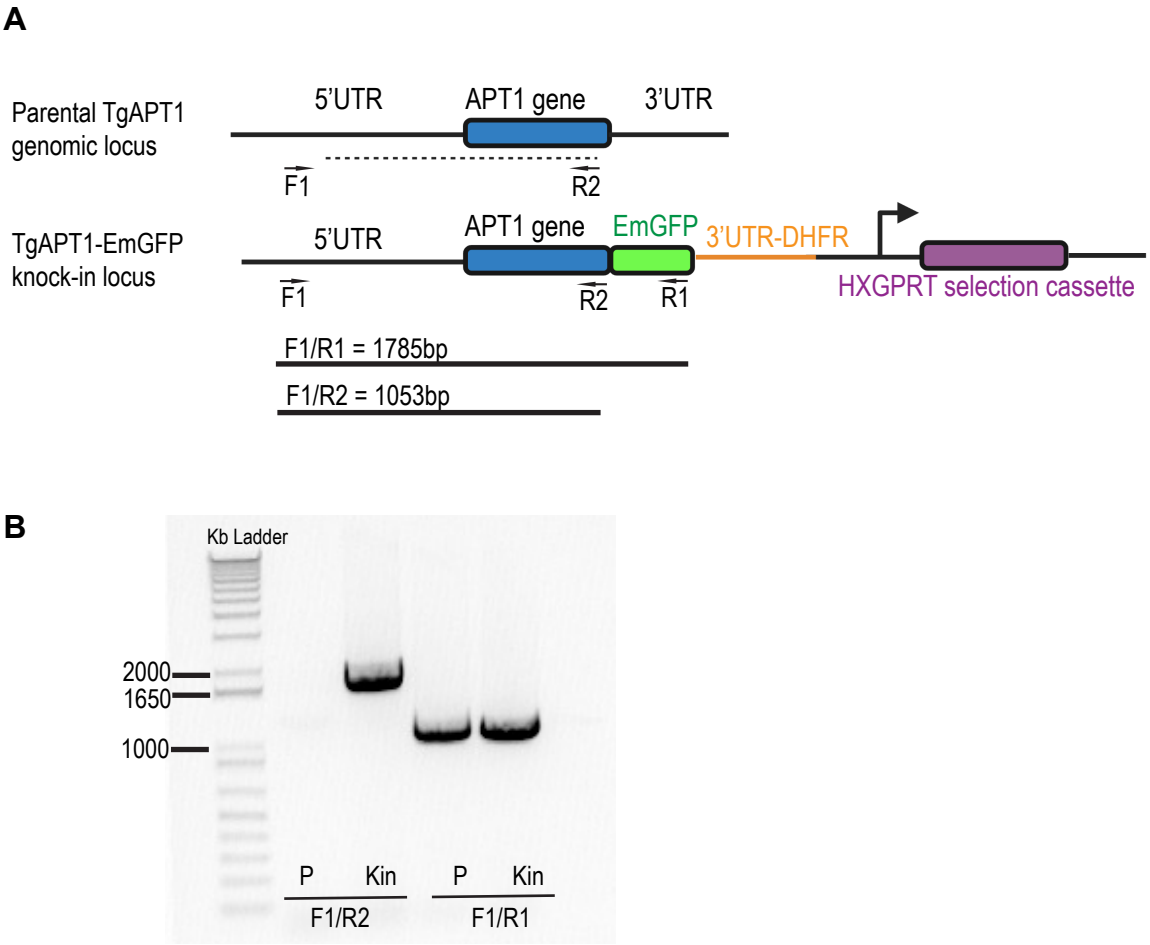

Figure S1: Creation of TgAPT1-EmGFP parasite line
(A) Schematic of TgAPT1 genomic locus in parental Ku80 parasites and TgAPT1-EmGFP knock-in parasites. Binding sites of primers used for diagnostic PCR are indicated. Expected PCR product size with F1 and R1 primers is 1785bp. Expected PCR product size for F1 and R2 primers is 1053bp. (B) Diagnostic PCR with F1/R2 and F1/R1 primer pairs using genomic DNA from parental Ku80 and APT1 knock-in parasites as a template.

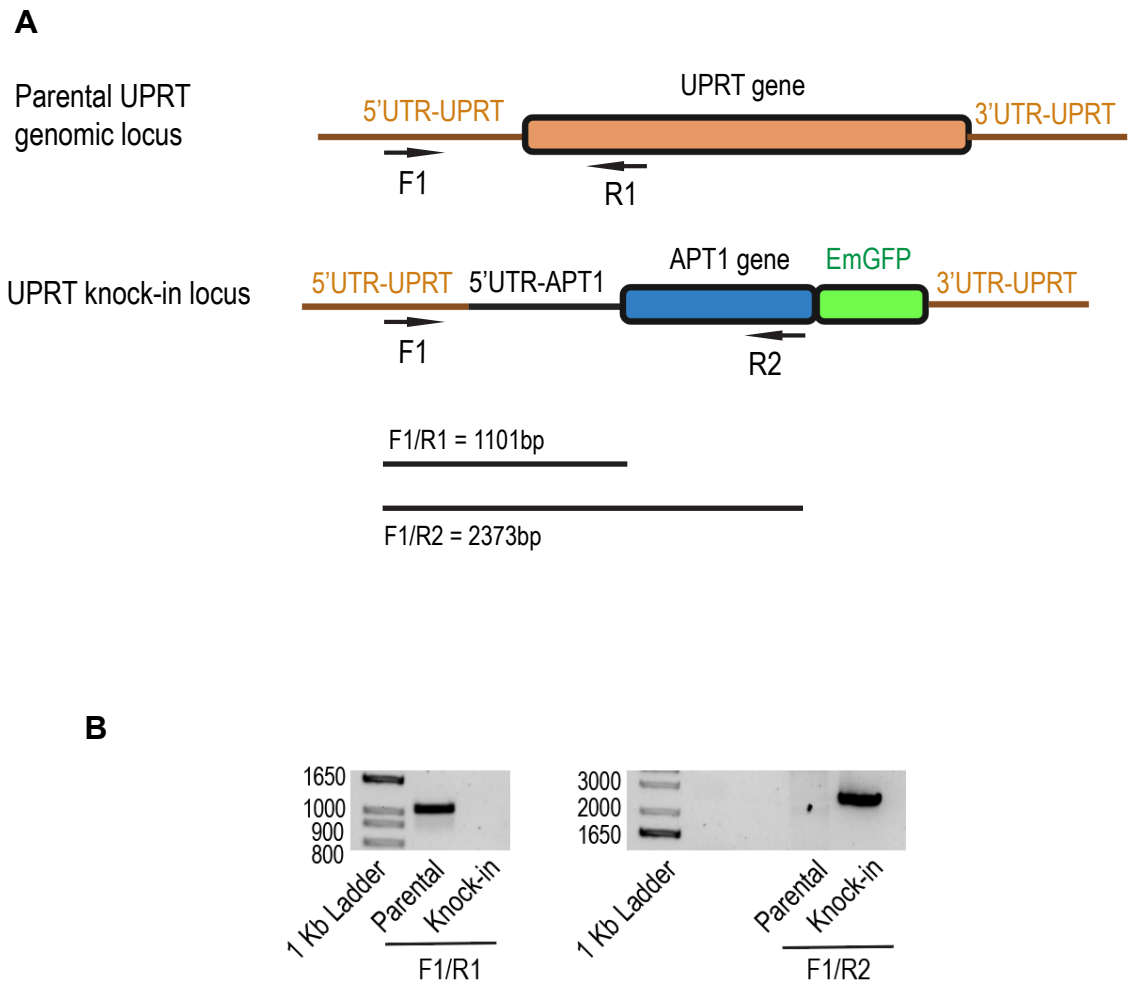

Figure S2: Creation of TgMyoF-AID: TgAPT1-EmGFP parasite line
(A) Schematic of UPRT genomic locus in parental TgMyoF-AID parasites and TgMyoF-AID:TgAPT1-EmGFP knock-in parasites. Binding sites of proteins used for diagnostic PCR are indicated. Expected PCR product size with F1 and R1 primers is 1101bp. Expected PCR product size for F1 and R2 primers is 2373bp. (B) Diagnostic PCR with F1/R1 and F1/R2 primer pairs using genomic DNA from parental and knock-in parasites as a template.

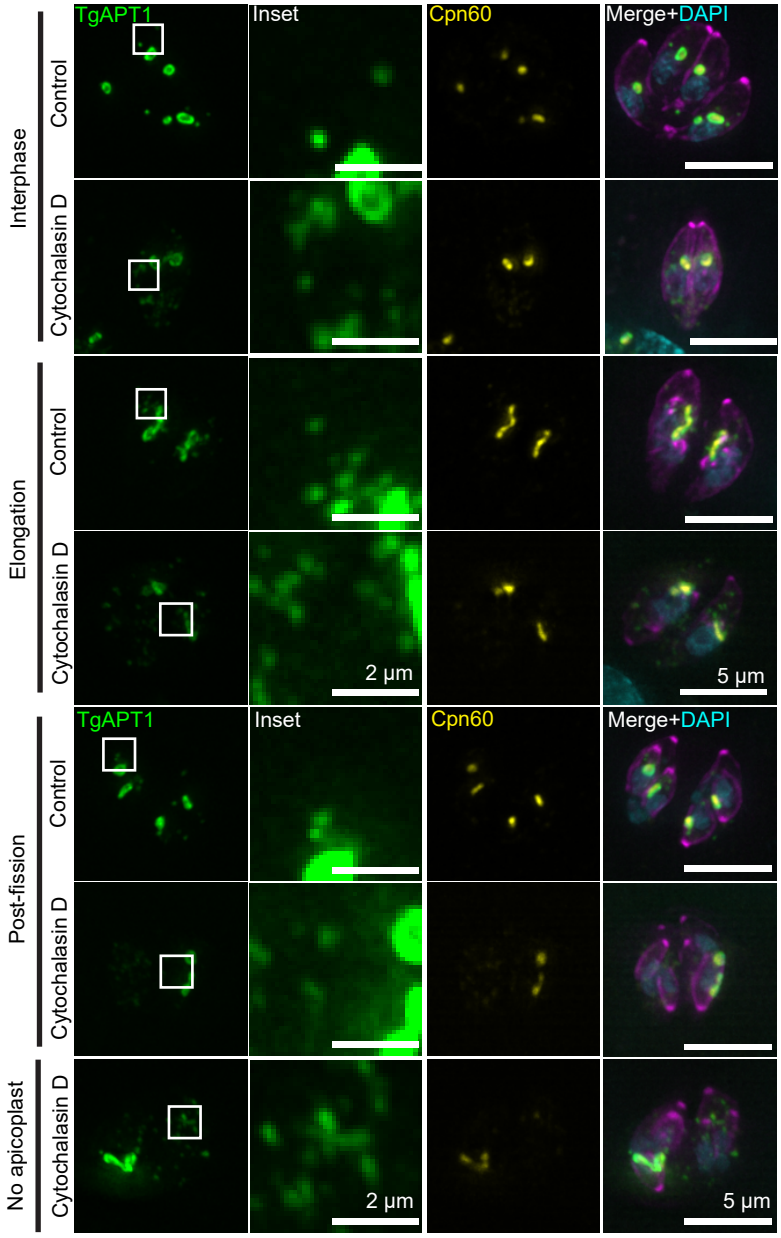

Figure S3: Actin depolymerization with cytochalasin D causes an accumulation of TgAPT1 vesicles in the cytosol

Fluorescent images of TgAPT1-EmGFP parasites treated with DMSO (control) or 0.2 mM cytochalasin D treated for 12 hours that were categorized as interphase, elongation and post-fission stages of the apicoplast division cycle. Parasites were fixed and stained with anti-Cpn60 antibody (a marker for the apicoplast shown in yellow) and DAPI (cyan). Panels are maximum intensity projections of deconvolved images. Scale bar represents 5 µm. White box indicates area used to make inset. Inset: Brightness and contrast of insets was adjusted to facilitate visualization of dimmer TgAPT1 vesicles. Inset scale bar represents 2 µm.

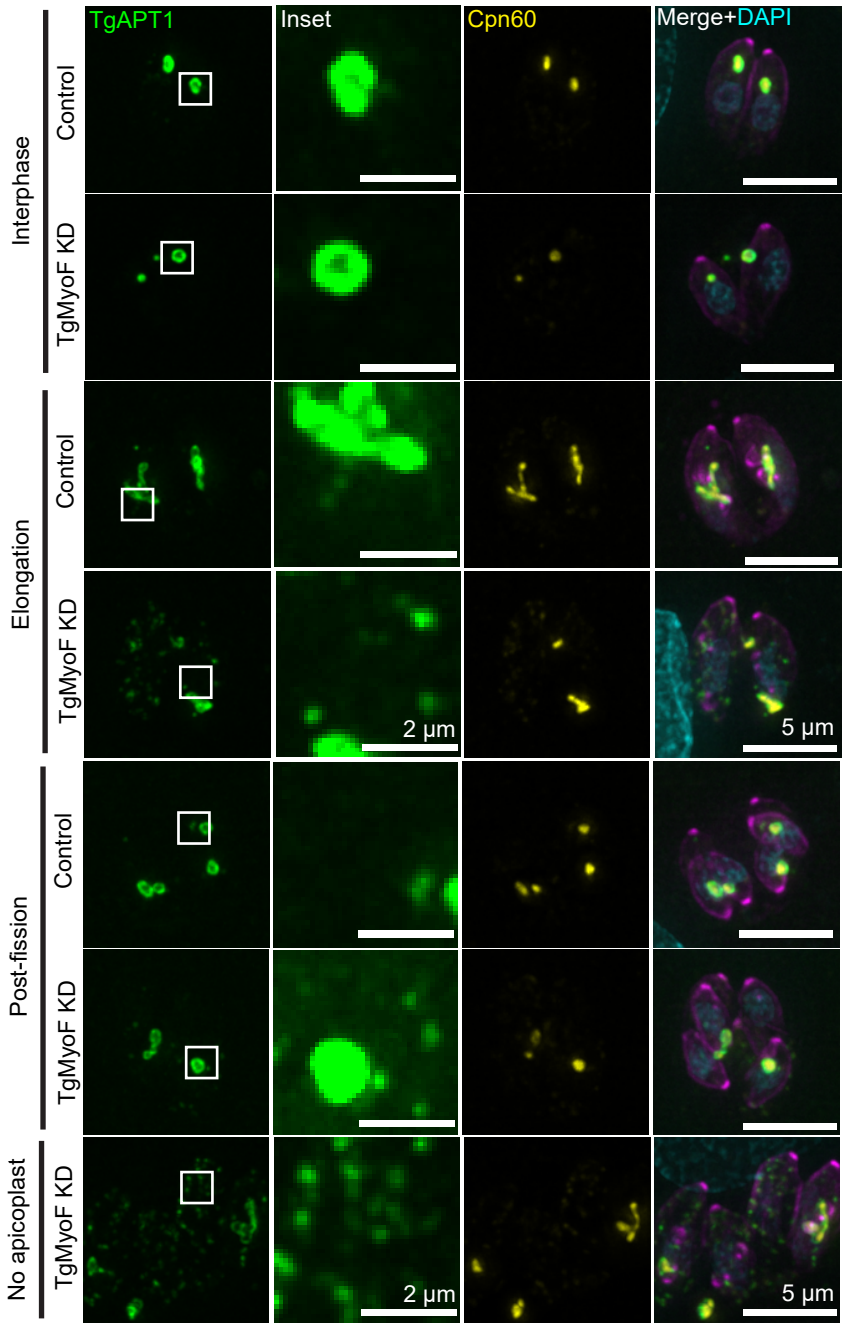

Figure S4: TgMyoF knockdown causes an accumulation of TgAPT1 vesicles in the cytosol

Fluorescent images of TgMyoF-mAID; TgAPT1-EmGFP parasites treated with ethanol (control) or 500 M IAA treated for 15 hours and then categorized as being in the inter-phase, elongation and post-fission stages of the apicoplast division cycle. Parasites were fixed and stained with anti-Cpn60 antibody (a marker for the apicoplast shown in yellow) and DAPI (cyan). Panels are maximum intensity projections of deconvolved images. Scale bar represents 5 µm. White box indicates area used to make inset. Inset: Brightness and contrast of insets was adjusted to facilitate visualization of dimmer TgAPT1 vesicles. Inset scale bar represents 2 µm.

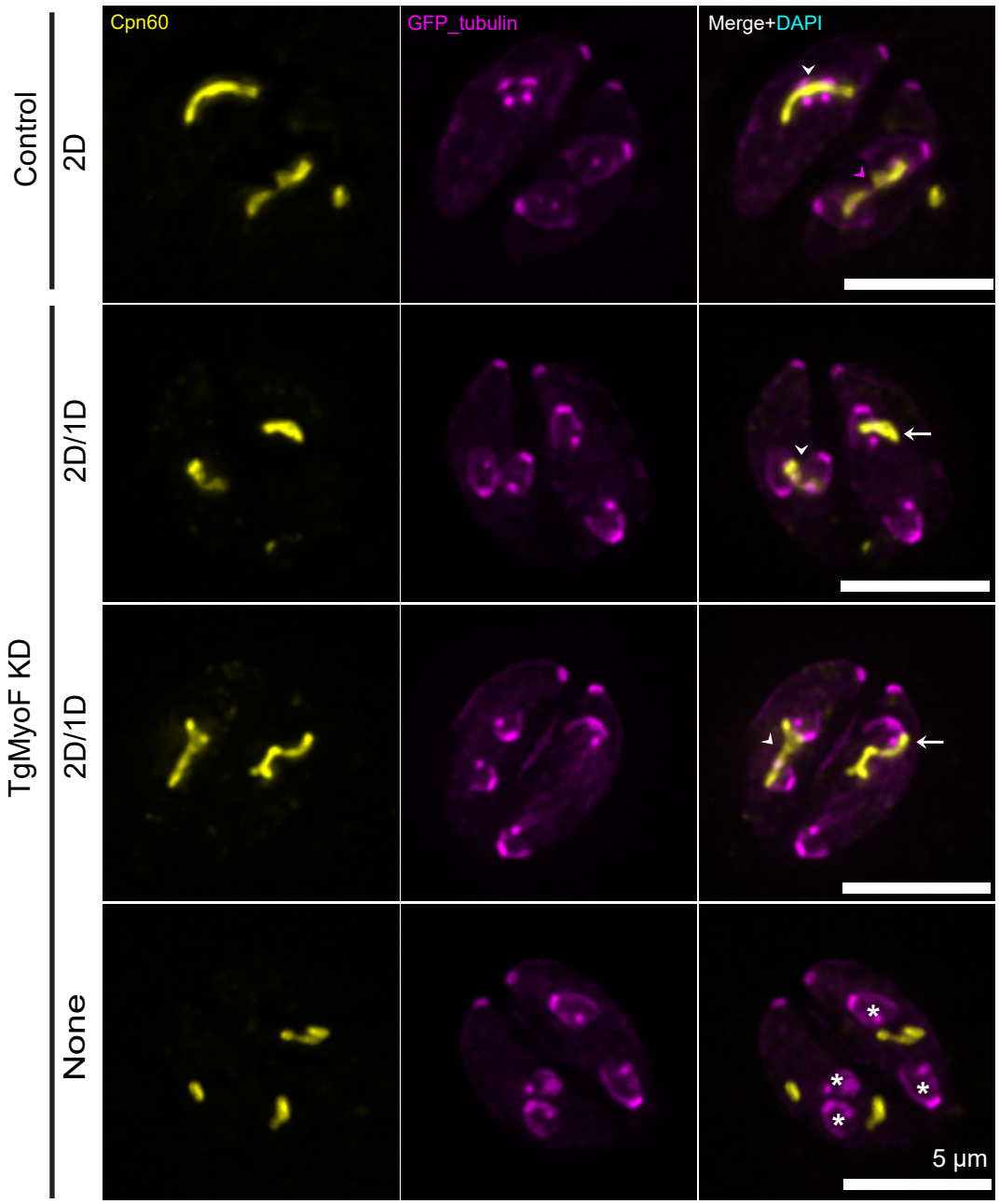

Figure S5: TgMyoF knockdown results in asymmetric localization of elongated apicoplast to daughter parasites.
Maximum intensity projection of deconvolved fluorescent images of TgMyoF-AID parasites treated with ethanol or IAA. Parasites are expressing eGFP-tubulin (magenta) stained with anti-Cpn60 antibody (yellow). Control parasites show that the elongated apicoplasts are in proximity to the daughter parasites (white arrowheads). Later in division, the tips of the elongated apicoplast are localized with the growing daughters (magenta arrowheads). Upon TgMyoF KD, there is an asymmetric localization of the elongated apicoplast to one of the daughter cells (white arrow). Parasites where the apicoplast association with the daughters appears normal is indicates with a white arrowhead. In some parasites the apicoplast is not associated with either daughter (indicated with an asterisk). Scale bar represents 5 μm.

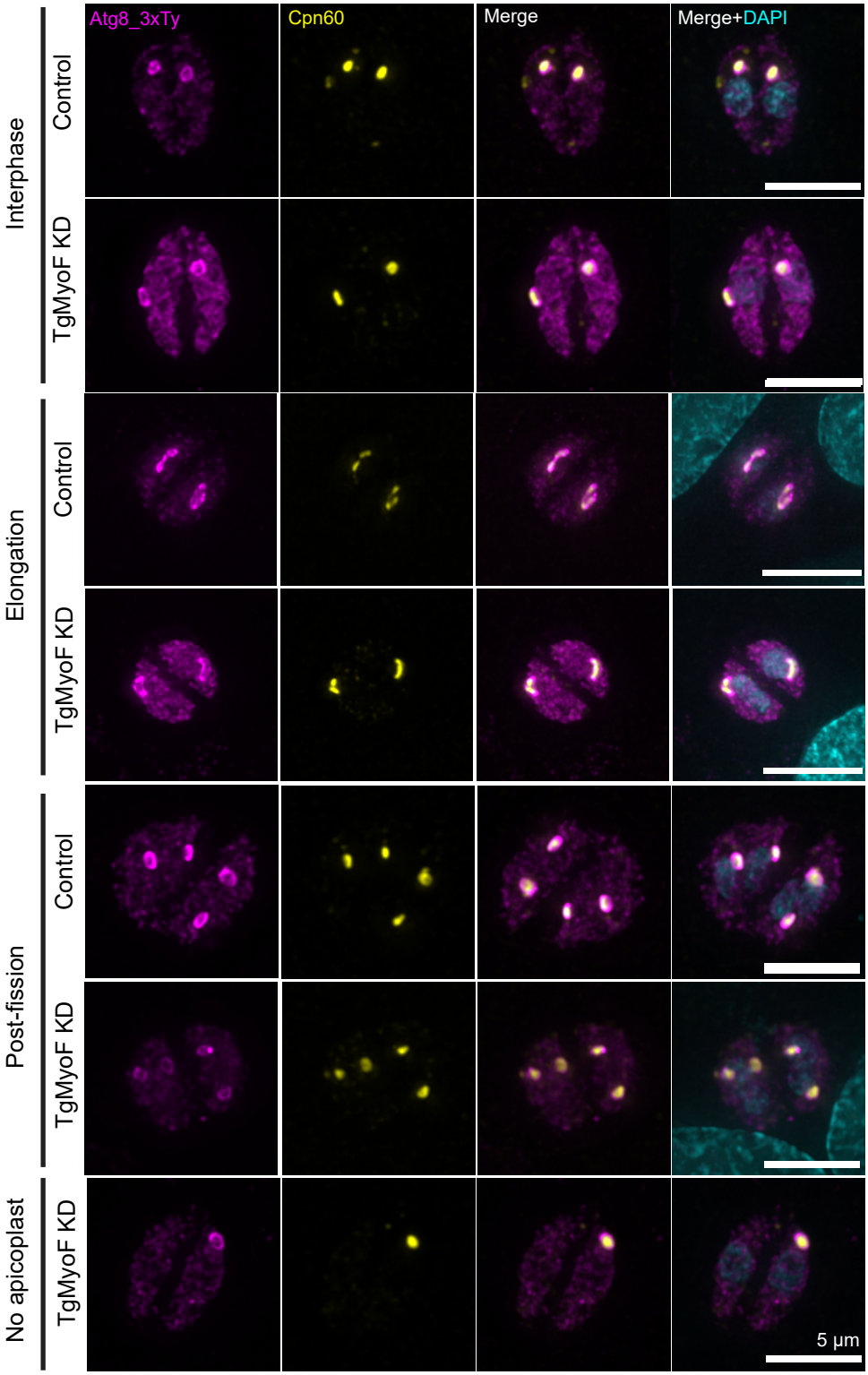

Figure S6: TgMyoF knockdown does not disrupt ATG8 association with the apicoplast. TgMyoF-mAID parasites ectopically expressing 3xTy-Atg8 under the control of the Atg8 promoter were grown for 12 hours before treatment with ethanol (control) or IAA (TgMyoF KD) for 6 hours. Cell were stained with anti-Ty (magenta) and anti-Cpn60 antibodies (yellow), and DAPI (cyan). Maximum intensity projections of deconvolved images of parasites during interphase, elongation and post-fission are shown. Scale bar represents 5 µm

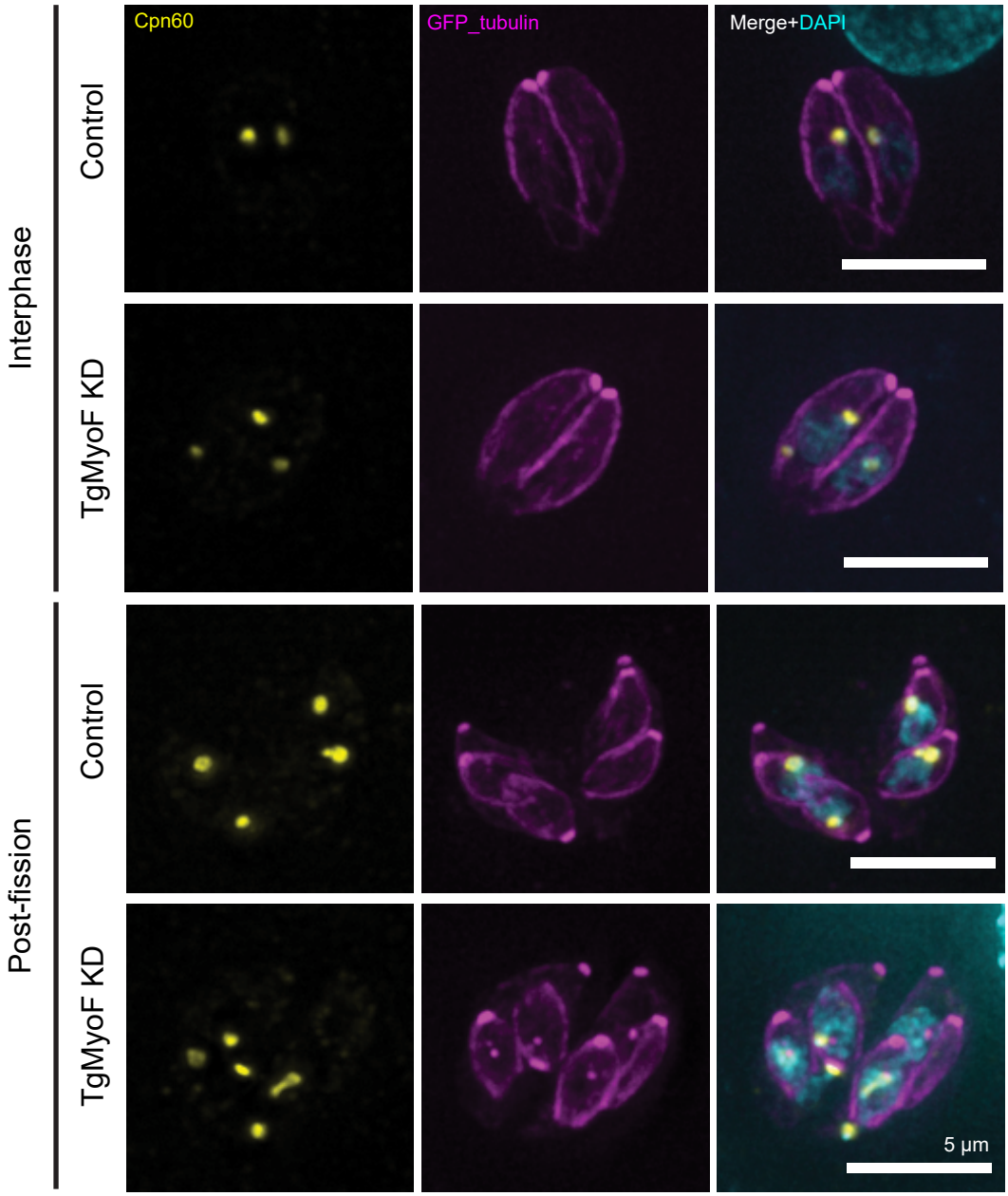

Figure S7: TgMyoF knockdown did not lead to changes in apicoplat morphology in interphase or post-fission stages of apicoplast division.
TgMyoF-mAID parasites expressing eGFP-tubulin (magenta) grown for 12 hours before treatment with ethanol (control) or IAA (TgMyoF KD) for 6 hours. Parasites with an anti-Cpn60 antibody (yellow) and DAPI (cyan). Parasites in interphase and post-fission stages of apicopalst divison are shown. Scale bar represents 5 µm.

Table 1. List of Plasmids used in this study

Plasmid Name	Purpose	Reference
pTKOII_APT1_EmGFP	Endogenous tagging of APT1EmGFP genomic locus	This study
pUPRT_APT1_EmGFP_3'UPRT	Expression of APT1-EmGFP from UPRT locus	This study
pUPRT_MyoFp_mCherry_MyoFcds_3'UPRT	Expression of mCherry-MyoF from UPRT locus	Unpublished plasmid
pAtg8_3xTy_Atg8	Fluorescent labeling of Atg8 subcloned from ptub_tdtomato_Atg8 (Leveque et al., 2015 PMID: 26507233)	This study
pmin_Centrin1_GFP	Fluorescent labeling of centrosomes	Hu K. 2008; PMID: 18208326
ptub_mcherry_ tubulinA1	Fluorescent labelling of parasite periphery and daughters	Hu et al., 2002; PMID: 11901169
ptub_eGFP_tubulinA1	Fluorescent labelling of parasite periphery and daughters	Hu et al., 2002; PMID: 11901169

Table 2 List of primers used in this study

Primer Name	Sequence	Purpose
TgAPT1 F1	AAACGACGGCCAGTGAGCGCGCCCACCGCGGTGGCCTAGGcctcgcgcgcgttcgtccgg	Gibson Primer (F) for inserting APT1 gene into pTKOII//EmGFP Plasmid
TgAPT1 R1	TGAACAGCTCCTCGCCCTTGCTCACGAGTCCGGAAGATCTtccgtacttggtcttcgaga	Gibson Primer (R) for inserting APT1 gene into pTKOII//EmGFP Plasmid
TgAPT1 promoter F1	TACCACTTCGCTTCCCTGTC	PCR Confirmation of integration of APT1-EmGFP into the endogenous locus
APT1 CDS R	TCCGTACTTGGTCTTCGAGAGA	PCR Confirmation of integration of APT1-EmGFP into the endogenous locus
EmGFP R	TTACTTGTACAGCTCGTCCATG	PCR Confirmation of integration of APT1-EmGFP into the endogenous locus
5'-APT1-UPRT-F	CGTATTCCTTTTTTCGTCGGACCTTTCCACAGGGCCTAGGcctcgcgcgcgttcgtccgg	Gibson Primer (F) for inserting APT1 gene into pTKOII//mcherryMyoF Plasmid
3'-APT1-UPRT-R	ATTCCGTCAGCGGTCTGTCAAAAAAACTAGAGACCTTAAGttacttgtacagctcgtcca	Gibson Primer (R) for inserting APT1 gene into pTKOII/mcherry MyoF Plasmid
5'-UPRT F	TTTTCCTGTTTTCGTCGTCATC	Creation of CrispR-HR Oligo and PCR Confirmation of integration of APT1-EmGFP into the UPRT locus
3'-UPRT R	TACCACTTCGCTTCCCTGTC	Creation of CrispR-HR Oligo
UPRT-Intron R	AGAGAGTTGAGAACAGGCTTC	PCR Confirmation of integration of APT1-EmGFP into the UPRT locus
Atg8 promoter F	AAGTGGCGAAACCCTCGGCAGTGCCTTGAAAAGAGGCGCCatgtttttgccctgcggcat	Replacement of pTub with pATG8 to create pATG8-ATG8-tdTomato
Atg8 promoter R	TGACCTCCTCGCCCTTGCTCACCCTAGGCATATGAGATCTgtttttcaagacggcgaata	Replacement of pTub with pATG8 to create pATG8-ATG8-tdTomato
3xTy F	tattcgccgtcttgaaaaacacctaggATGGAGGTCCATACTAACCA	Replacement of tdTomato with 3xTy to create pATG8-ATG8-3xTy1
3xTy R	AGGACACTTCGTCGCGAATCGATGGCATCCCATGAGATCTatcaagggggtcttggttcg	Replacement of tdTomato with 3xTy to create pATG8-ATG8-3xTy1

Table S3: List of gene accession numbers associated for proteins in this study

Gene Name	**ToxoDB Accession Number**
TgMyoF	TgME49_278870
TgAPT1	TgME49_261070
TgATG8	TgME49_254120
TgCpn60	TgME49_240600
Centrin 1	TgME49_247230

Table 3 List of antibodies used in this study

Primary Antibody	Catalog #	Dilution	Reference/Source
Rabbit anti-Cpn60	Custom	1:2000	Dr. Boris Striepen; University of Pennsylvania
Mouse anti-IMC1	Custom	1:750	Dr. Gary Ward; University of Vermont
Mouse anti-Ty1	Custom	1:1000	Dr. Christopher deGraffienried; Brown University
Secondary Antibody	**Catalog #**	**Dilution**	**Reference/Source**
Goat anti-mouse Alexa Fluor 488	A11006	1:500	Invitrogen
Goat anti-mouse Alexa Fluor 546	A11030	1:1000	Invitrogen
Goat anti-rabbit Alexa Fluor 647	A21245	1:5000	Invitrogen